Research Square

Preprints are preliminary reports that have not undergone peer review.
They should not be considered conclusive, used to inform clinical practice,
or referenced by the media as validated information.

Targeting MDR Pseudomonas aeruginosa biofilm with an evolutionary trained bacteriophage cocktail exploiting phage resistance trade-offs

Fabian Kunisch
Westfälische Wilhelms-Universität Münster
Jeroen Wagemans
KU Leuven https://orcid.org/0000-0002-2185-5724
Selma Yildirim
Berlin Institute of Health at Charité – Universitätsmedizin Berlin
Benjamin Chan
Yale University
Christoph Schaudinn
Robert Koch Institute
Rob Lavigne
KU Leuven https://orcid.org/0000-0001-7377-1314
Paul Turner
Yale University https://orcid.org/0000-0003-3490-7498
Michael Raschke
Westfälische Wilhelms-Universität Münster
Andrej Trampuz
andrej.trampuz@charite.de

Charité – Universitätsmedizin Berlin
Mercedes González Moreno
Charité – Universitätsmedizin Berlin

Article

Keywords:

Posted Date: June 19th, 2023

DOI: https://doi.org/10.21203/rs.3.rs-2545888/v1

License: This work is licensed under a Creative Commons Attribution 4.0 International License.
Read Full License

Additional Declarations: Yes there is potential Competing Interest. One co-author declares a conflict of interest as cofounder of a company that seeks to develop phages for human therapy. The other authors declare no competing interests.

Version of Record: A version of this preprint was published at Nature Communications on October 3rd, 2024. See the published version at https://doi.org/10.1038/s41467-024-52595-w.

Targeting MDR *Pseudomonas aeruginosa* biofilm with an evolutionary trained bacteriophage cocktail exploiting phage resistance trade-offs

Abstract

Spread of multidrug-resistant *Pseudomonas aeruginosa* strains threatens to render currently available antibiotics obsolete, with limited prospects for the development of new antibiotics. Lytic bacteriophages (phages), the natural predators of bacteria, represent a path to combat this threat. *In vitro* directed evolution is traditionally applied to expand the phage host range or increase bacterial suppression in planktonic cultures. However, while 80% of human microbial infections are biofilm-associated, research towards targeted improvement of phages' ability to combat biofilms remains scarce. Here, we describe an *in vitro* evolution assay that improves multiple phage parameters in parallel, while optimizing phage cocktail design by exploiting a bacterial phage resistance trade-off. The obtained evolved phages show an expanded host spectrum, improved antimicrobial efficacy under isothermal microcalorimetric monitoring and enhanced antibiofilm performance, as determined by RT-qPCR. Our two-phage cocktail revealed further improved antimicrobial efficacy without incurring dual-phage-resistance in treated bacteria. We anticipate this assay will allow a better understanding of phenotypic-genomic relationships in phages and enable the training of phages against other desired pathogens. This, in turn, will strengthen phage therapy as a treatment adjunct to improve clinical outcomes of multidrug-resistant bacterial infections.

Introduction

Worldwide emergence and spread of multidrug-resistant (MDR) *Pseudomonas aeruginosa* strains represents a critical public health threat, since currently available antibiotics are losing their efficacy. Furthermore, the development of new antibiotics is in decline, reinforcing the need for new approaches to treat infections with antibiotic-resistant strains[1-4]. As a ubiquitous Gram-negative pathogen, *P. aeruginosa* commonly causes opportunistic nosocomial infections, for instance, healthcare-associated pneumonia, bacteraemia and infections of the urinary tract[5]. Harnessing the selective permeability of its outer membrane, the ability to expel antibiotics from its cell through efflux systems, mutational changes and horizontal gene transfer, *P. aeruginosa* is intrinsically resistant to several antibiotics[6]. Finally, transiently adapting gene and/or protein expression levels can cause changes in its motility, induce a persister state, or biofilm growth, generally conferring additional protection[6,7].

Biofilms are highly organized bacterial communities that adhere to one another and/or to surfaces and are embedded within a matrix of self-produced extracellular polymeric substances (EPS). Biofilms cause up to 80% of human microbial infections[8-11]. Accounting for around 85-90% of the total organic fraction[12] in biofilms, the EPS of *P. aeruginosa* comprises exopolysaccharides (Pel, Psl, alginate), nucleic acids (external DNA) and proteins (CdrA/LapA) [13,14]. This bacterial lifestyle protects the enclosed cells from desiccation, impedes mechanical removal and undermines the efficacy of antibiotics and disinfectants[15,16]. In addition, biofilms provide a safe haven from the innate and adaptive immune system, making them difficult to erradicate[17].

Bacteriophages (phages) have received renewed attention over the last decade as alternative antimicrobial agents to treat *P. aeruginosa* biofilms[18,19]. Lytic phages, naturally occurring viruses infecting bacteria, ultimately lyse their host cells. Three principal factors make phages promising antimicrobial agents for bacterial biofilm infections. First, once a phage infects and replicates within a bacterial biofilm cell, it causes a localised increase of infectious progeny. They subsequently spread further into the biofilm, thereby infecting, and lysing other bacterial cells. This in turn leads to the destabilization of the biofilm population and impairs any regeneration attempts. Second, various virion-associated depolymerizing enzymes[20-24] and lysins[25] help phages reach and disintegrate their bacterial hosts and associated biofilm matrix[26-29]. Last, some phages have the ability to infect biofilm persister cells (dormant, non-dividing cells that exhibit increased tolerance to antimicrobials), which are killed once they revert to normal growth, as the phages initiate the lytic replication cycle[30], thus decreasing the risk of infection relapse.

Faced with the challenge of evolved bacterial phage resistance in a therapeutic setting, two main approaches have been a focus. Besides their expanded host range, phage cocktails – mixtures of several phages – exert distinct selection pressures on the target strain and thus reduce the probability of simultaneously evolved resistance towards multiple phages[31-33]. Phage training aims to select phages that show an improved circumvention of bacterial defence mechanisms due to *de novo* mutations or recombination events[34-36]. Furthermore, there have been directed evolution approaches building on the inherent properties of phages to improve phage killing efficacy in terms of, for instance, expanded host range[37], phage thermal stability[38,39] or greater bacterial suppression[34,40].

In our study, we integrated the combined improvement of the phages' host spectrum, antimicrobial and antibiofilm capabilities by implementing an *in vitro* directed evolution approach against biofilm bacteria. To further improve the efficacy of evolved phages against MDR *P. aeruginosa* strains, we designed a resistance-adapted phage cocktail. This study provides a phage training platform and helps to better understand evolutionary genetics of interactions between evolving phages and bacteria and enables us to identify different genomic parameters conferring enhanced phage efficacy.

Results

Training phages on biofilms by serial passage in a directed evolution assay

To overcome the challenges that *P. aeruginosa* biofilms pose to infection management, we developed an evolutionary serial passage assay (Figure 1), that utilizes a directed evolution approach, to simultaneously improve several phage infectivity parameters. This assay was implemented using four lytic *P. aeruginosa* phages, belonging to three distinct genera, which were trained on eight *P. aeruginosa* strains, which also display diversity in genomic phylogenetics, antibiotic resistance, and biofilm formation traits (Figure 2a; Extended Data Figure E1; Supplementary Data S1). During each round, pre-established (24 h) biofilms of ancestral bacteria were incubated with a mixture of the phages under isothermal microcalorimetric heat production control. After each passage, all samples showing a heat reduction greater than 75% (compared to growth control) were pooled and the undiluted phage samples (always included) together into the new phage mixture. In total, 30 rounds of evolution were performed.

Throughout the evolution assay (round 1, 5, 10, 15, 20, 25, and 30), we observed an overall increased calorimetric heat reduction after 8 h in consecutive rounds of evolution for each individual strain (Extended Data Figure E2), except for Paer33. This improved activity was further confirmed at lower phage concentrations, achieving heat reductions equivalent to those from higher concentrations in previous rounds. Ultimately, we observed how 10 PFU/ml (plaque forming units/ml) of the phage mixture resulted in reductions of 68.9% and 81.7% for the strains Paer57 (Extended Data Figure E2d; round 30) and Paer03 (Extended Data Figure E2b; round 25), respectively.

When focusing on the entire monitoring period (24 h) instead, we observed that four strains (PAO1, Paer03, Paer57 and Paer84) co-incubated with the phage mixture reached heat levels equivalent to those from their respective growth controls (Extended Data Figure E2). However, it should be noted that a delay in reaching the heat plateau was observed. Presumably, this delay corresponds to the time of bacterial suppression before phage resistance emerged. Among the analysed time points, the duration of this initial heat suppression is strain-specific and could reach up to 18.27 h (Paer57, round 5, 3.07 x 10^7 PFU/ml), excluding strains Paer09 and Paer85. In the case of Paer09, from round 3 onward, we observed a complete heat suppression (≥75%) for the entire monitoring period in the undiluted phage sample. Lower phage concentrations could still prevent the sample from reaching the growth control plateau level (with exceptions in samples containing a higher phage dilution). Similarly, the Paer85 heat production was continuously suppressed and did not reach growth control plateau levels.

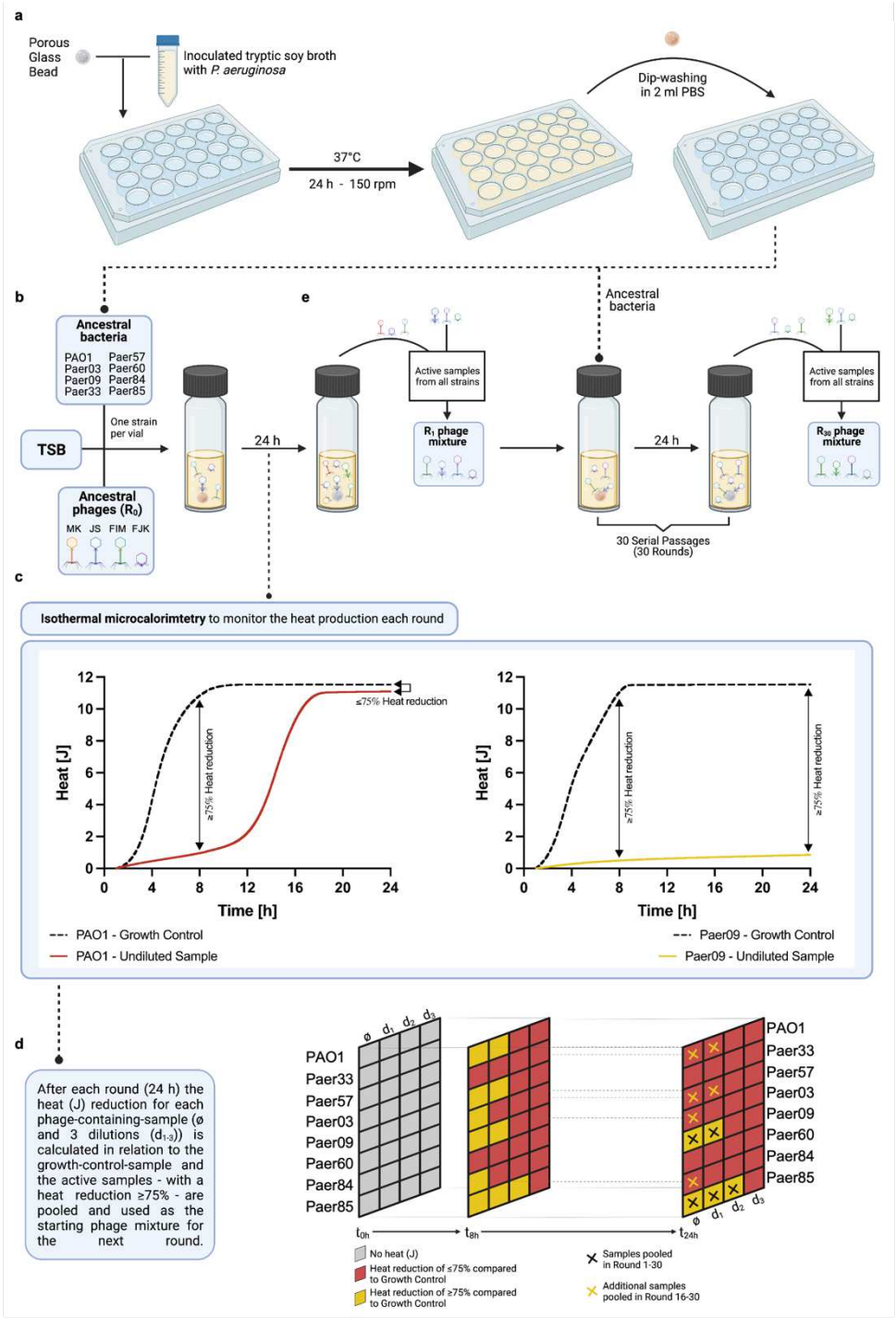

Fig. 1: Experimental design of the antibiofilm evolution assay.

Experimental setup of the evolution assay to extend the host range and improve the antimicrobial and antibiofilm activity of bacteriophages. **a**, Biofilm formation on porous glass beads by incubation with *P. aeruginosa* in tryptic soy broth (TSB) under agitation and 37 °C. Dip-washing of beads with 24 h pre-established biofilm in sterile phosphate-buffered saline (PBS) before transferal into the calorimetric

ampules. **b**, Representation of one calorimetric ampule containing a 24 h pre-stablished biofilm bead of one *P. aeruginosa* strain in TSB and the phage mixture at round 0 (R0) containing the four ancestral phages. A total of 43 ampules (five per each strain and three sterility controls) were used during each round of evolution. **c**, Heat production (J) was recorded for each individual ampule by isothermal calorimetry during 24 h. **d**, At the end of each round, the percentage heat reduction of phage-containing ampules relative to growth control ampules was determined at a 24 h (rounds 1-15) or 8 h (rounds 16-30) time point. Samples showing a heat reduction equal or above 75% (referred as active samples) were selected and pooled together with the undiluted phage samples (always included) into the new phage mixture. **e**, Across all eight bacterial strains, the undiluted and the active samples after each round were pooled together, creating the phage mixture that served as starting point for the next round, and hence was added to pre-stablished biofilm beads anew. In total, 30 rounds of evolution were performed.

Combined improvement of three phage infectivity parameters

Upon completion of the phage evolution assay, to compare the infectivity parameters of the untrained, unevolved genomic phage ancestors with the evolved phages, we isolated individual phages from the phage mixtures of evolution round fifteen and thirty. For direct comparison of the phages' host range, antimicrobial biofilm activity and antibiofilm efficacy we employed soft agar overlay spot assays, co-incubated pre-established biofilms with phages under isothermal microcalorimetry monitoring and determined the bacterial biofilm count reduction by real-time quantitative polymerase chain reaction (RT-qPCR).

Based on plaque morphology and host strain, we isolated 31 individual evolved phages from the phage mixtures (17 from round 15 and 14 from round 30). Of those, our analyses focused on a representative subset of ten: MK.R3-15/30, MK.R57-15/30, MK.R84-15/30, FIM.R60-15/30 and FJK.R9-15/30 named after the phage's genetic ancestor (e.g., MK), bacterial strain

of isolation (e.g., Paer57) and the round of evolution it was isolated (round 15 or 30). The representatives are unique phages descended from all four ancestral phages, showing distinct efficiency and host range in preliminary tests (data not shown). Similarly, from the 80 bacterial strains in our collection, three strains with distinct phage susceptibility profile were selected, two of which were included in the evolution assay (Paer09 and Paer57) and one that was not included (Paer36), as target strains for further analysis.

In terms of host range, each evolved phage could overcome the resistance of specific bacterial strains observed with the ancestral phage, while at the same time losing infectivity towards other strains (Figure 2b). In this manner, all but two (evolved phages of FIM), showed an extended host range compared to their ancestors (Figure 2c). Compared to its direct genomic ancestor (MK), phage MK.R57-30 showed the largest host range expansion. It could infect 11 additional strains, eight of which were initially not susceptible to any of the ancestral phages and three were susceptible to other phages but resistant to MK. This expansion enabled MK.R57-30 to infect 37.5% of all *P. aeruginosa* strains, a 20.0% increase compared to the ancestral phage FIM, which displayed the broadest host range among the ancestral phages. For the evolved phages, we calculated a 44.1% greater increase in infectivity among the eight bacterial strains included in the evolution assay than in the strains not included (Figure 2d).

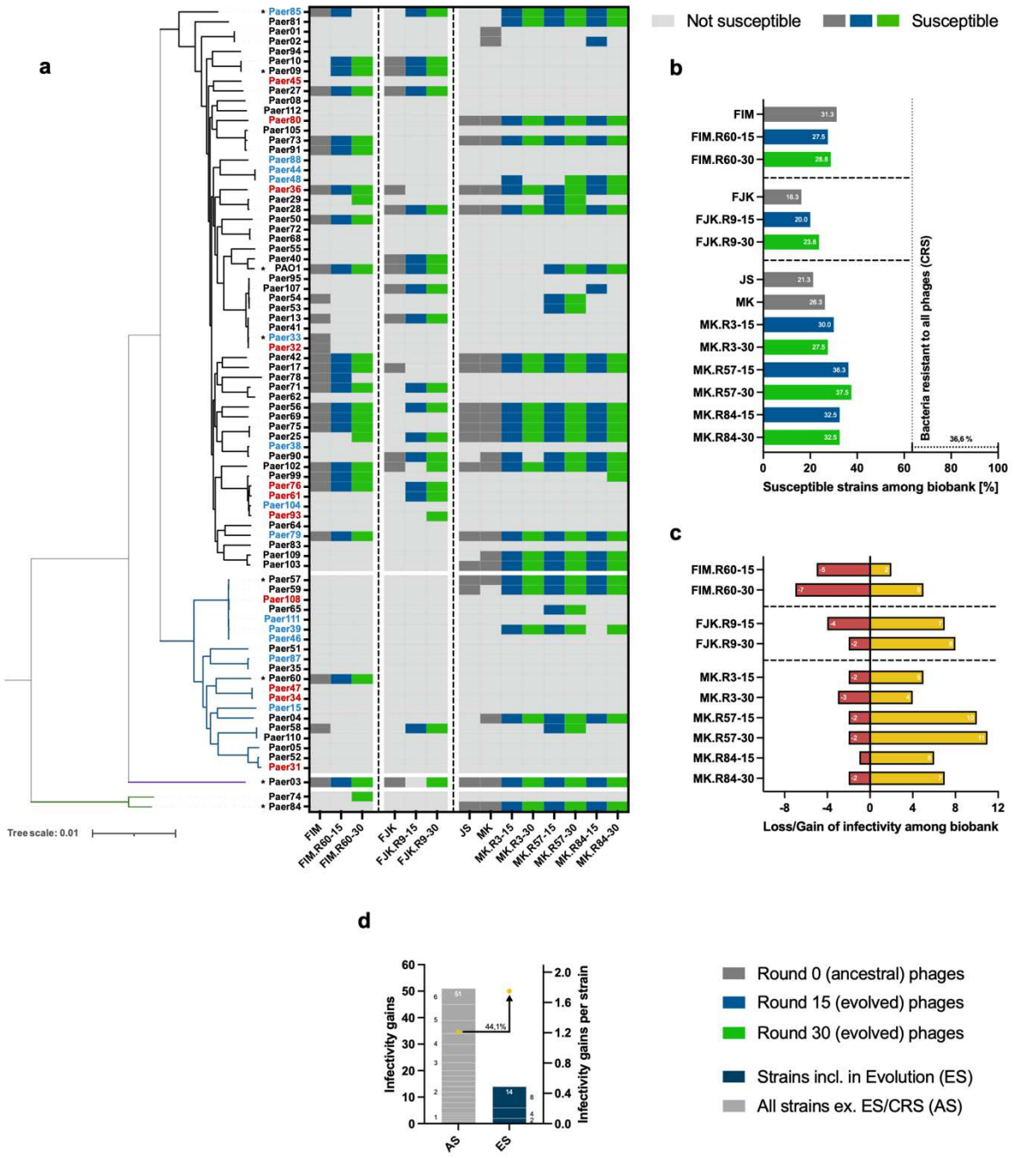

Fig. 2: Host range analysis of unevolved and evolved phages.

a, Phylogenetic tree of the collection of *P. aeruginosa* strains (biobank of 80 *P. aeruginosa* strains including information on their genomic clusters, antibiotic resistance and biofilm formation traits) encompassing four genomic clusters (Cluster 1, black branch, 71.3%; Cluster 2, blue branch, 25.0%; Cluster 3, violet branch, 1.3%; Cluster 4, green branch, 2.5%). Classification of each strain according to its resistance profile (4MRGN, red lettering; 3MRGN, blue lettering). Strains marked with an asterisk

(*) were included in the experimental evolution. Activity determination of the unevolved (dark grey) and evolved (R15, blue; R30, green) phages against the bacterial biobank by spot assay overlay (heat map). **b**, Percentual infectivity of each phage among the biobank. Vertical dotted line represents the percentage of strains in the biobank susceptible to at least one phage (62.5%). 37.5% (30 strains) of bacterial strains were not susceptible to any phage (CRS, completely resistant strains). **c**, Representation of the gain (yellow bar; bacterial strains susceptible to evolved phage but not to direct progenitor phage) and loss (red bar; bacterial strains susceptible to the direct progenitor phage but not to the evolved phage) of infective capability of each evolved phage with relation to its genomically closest unevolved progenitor. **d**, Representation of the cumulated infectivity gains of the evolved phages among the evolution strains (ES) or all strains (AS, excluding the ES and CRS). ES comprises the eight strains included in the evolution assay (stacked blue boxes corresponding to three strains, numbers at the side of the boxes indicate the infectivity gains on the according strain). AS comprises 44 strains (stacked grey boxes corresponding to 20 strains, numbers at the side of the boxes indicate the infectivity gains on the according strain) in the biobank from which the evolution strains (ES, eight strains) and the strains resistant to all phages (CRS, 30 strains) were excluded. For direct comparison of the cumulated infectivity gains among the two strain populations the cumulated values have been divided by the number of strains in each group (yellow circles).

Regarding the antimicrobial activity against pre-established biofilms, the evolved phages showed a higher suppressive effect on bacterial cells than their respective unevolved ancestral phages. In addition, the evolved phages could suppress bacterial heat production for a longer period before bacterial outgrowth occurred, presumably corresponding to emergence of phage resistance (Supplementary Table S1). When incubated with Paer09, the evolved phage FJK.R9-30 revealed a minimum heat flow of 11.6 µW, representing a 68.4% (p=0.0004) greater heat flow suppression compared to the ancestral phage FJK (36.6 µW) (Figure 3b). At the same time, phage FJK.R9-30 resulted in a 64.6% longer lag time than the ancestral phage (13.8 h vs. 22.7 h, p=0.0085). Ancestral phage MK showed a minimum heat flow of 77.2 µW, whereas the evolved phage MK.R57-30 reached a 96.5% (p=0.0053) greater reduction at 2.7 µW

(Figure 3f). With a 375.7% (p=<0.0001) longer lag time, MK.R57-30 suppressed the bacterial growth of Paer57 for 15.7 h (ancestral phage MK, 3.3 h) (Figure 3h). Against Paer36, a strain not included in the evolution assay, the evolved phage MK.R3-30 could both suppress bacterial heat production for longer (15.2 vs. 6.1 h, p=0.0105) and reduce heat flow to lower levels (20.3 vs. 80.4 µW, p=0.0369) than the corresponding unevolved ancestral phage (MK).

Across all tested strain-phage combinations, we could show that the phages evolved for thirty rounds demonstrated a greater antibiofilm activity with lower biofilm cell counts compared to their unevolved ancestors and, with one exception, than their counterparts evolved for fifteen rounds (Supplementary Table S2). After 6 h co-incubation of phage FJK.R9-30 and Paer09, the cell count was 74.9% (p=0.0010) lower compared to results from ancestral phage FJK (Figure 3a). Compared to the ancestral phage MK, the evolved phage MK.R57-30 showed a 99.7% (p=0.2473) and 86.7% (p=0.0431) greater cell count reduction of Paer57 biofilm cells after 6 and 24 h, respectively (Figure 3e). After 3 h of incubation (Paer57) phage MK.R57-30 resulted in a 58.7% (p=0.0032) lower cell count than phage MK.R57-15. Against Paer36 (not included in the evolution), the phage evolved for thirty rounds (MK.R3-30) outperformed the ancestral phage (MK) by 85.4% (p=0.0529) after 3 h of incubation. Similarly, after 6 h of incubation (Paer36) phage MK.R3-30 showed an 85.0% (p=0.0067) greater biofilm cell count reduction than the phage MK1.R3-15 (Figure 3i).

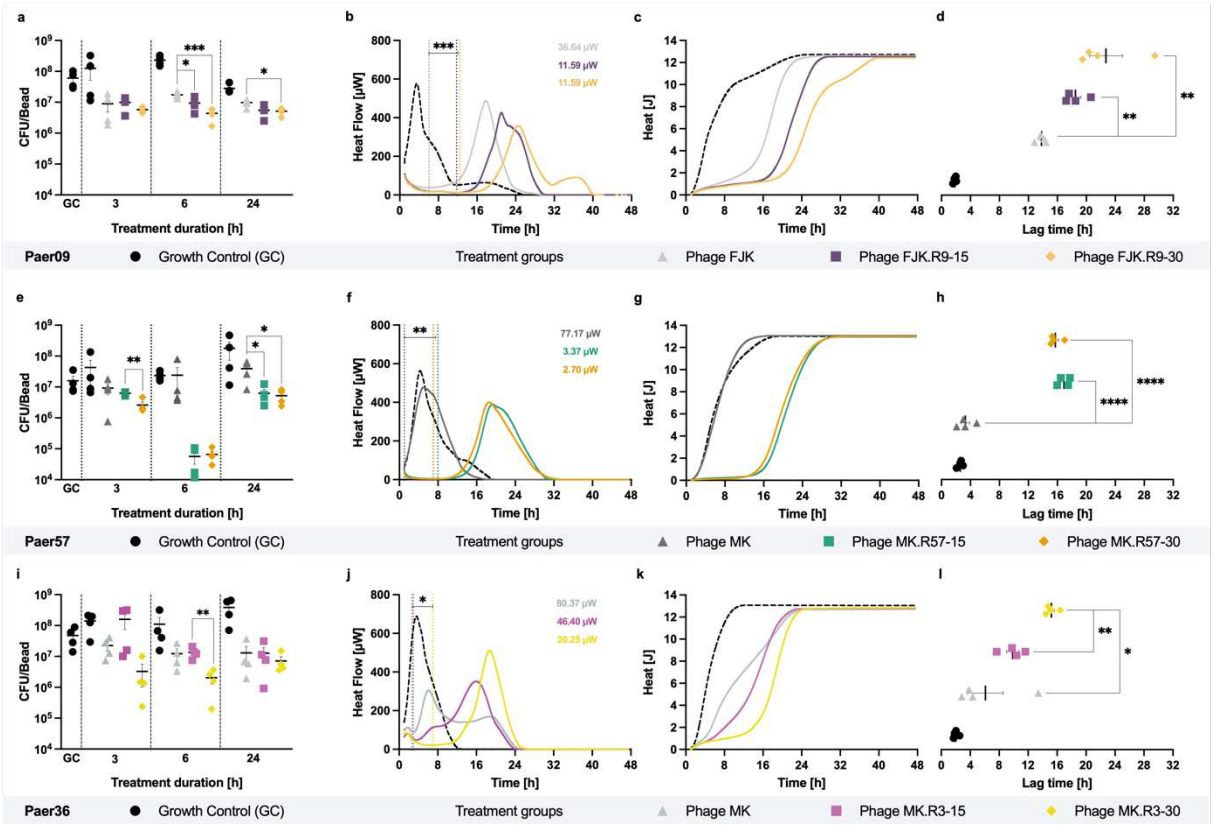

Fig. 3: Antibiofilm and antimicrobial activity of unevolved and evolved phages.

a, qPCR-determined bacterial load (CFU/bead) of 24 h pre-established Paer09 (included in the evolution) biofilm without treatment (GC) and after co-incubation (3, 6 and 24 h) with phage FJK (unevolved), phage FJK.R9-15 (15 rounds of evolution) and phage FJK.R9-30 (30 rounds of evolution). **b**, Heat flow (µW) curves measured for 48 h of Paer09 biofilm co-incubated with phage FJK, phage FJK.R9-15, phage FJK.R9-30 or without phage (GC, dashed line). Vertical dotted lines indicate the minimum heat flow (µW values shown on the right of the graph) detected in each treated sample, related to the highest suppressive effect of the phage on bacterial cells. **c**, **d**, Respective heat (J) curves of phage treated Paer09 biofilm and the calculated suppression time for each tested condition. **e, f**, **g**, **h**, Identical setup for the tested strain Paer57 (included in the evolution) treated with phage MK, phage MK.R57-15, phage MK.R57-30 or without phage (GC). **i**, **j**, **k**, **l**, Identical setup for the tested strain Paer36 (not included in the evolution) treated with phage MK, phage MK.R3-15, phage MK.R3-30 or without phage (GC).

All experiments were conducted in fourfold and the curves (b, c, f, g, j, k) display the mean. The error bars represent the standard error of the mean. The statistical analysis was conducted by unpaired two-

tailed Student's *t* test and *p*-values were indicated by an asterisk (*, p=<0.05; **, p=<0.01; ***, p=<0.001; ****, p=<0.0001).

Directed evolution primarily drives mutational events in structure-associated genes

To better understand the evolutionary mutational changes that underpin the improvement of our evolved phages' infectivity, we sequenced all unevolved and evolved phages. By comparing the genomes of the phages improved over fifteen and thirty rounds with their genetic ancestors, we anticipated to find mutations located among structural protein coding genes associated with host recognition and the degradation of extracellular polymeric substances.

By directed evolution, phages FJK.R9-15 and FJK.R9-30 lost a part of the early gene region and present single-nucleotide polymorphisms (SNP) in their genome leading to missense mutations in two genes encoding a L-glutamine-D-fructose-6-phosphate-aminotransferase and an amidoligase, as well as mutations in four genes encoding structural proteins (Figure 4a). It is remarkable that, although not in the same position, all SNPs for both evolved phages are clustered towards the same genes. For the structural proteins, gp52 contains a peptidoglycan transglycosylase (HHPred; $7.5x10^{-41}$ e-value) domain, that can degrade the bacterial cell wall peptidoglycan layer during the phage infection step[41]. Likewise, gp62 has similarity with tail tubular protein A (TTPA) of *Klebsiella* phage KP32 (HHPred; $8.6x10^{-5}$ e-value) which has EPS depolymerase activity[42]. The tertiary structure of gp62 predicted with ColabFold (Figure 4d) illustrates the mutation of amino acid 98 from a cysteine to a phenylalanine. Compared to TTPA, gp62 contains an additional α-helix close to the β-sheets, in which the mutation

occurred, which could therefore lead to a conformational change in the β-sheets region and, consequently, a change in catalytic activity.

Both phages FIM.R60-15 and FIM.R60-30 contained SNPs in tail fiber coding genes (gp42 and gp43). The phage evolved for thirty rounds displayed an additional SNP in gene gp8, encoding a hypothetical protein, and gp44, containing a tail fiber assembly domain (HMMER; $3.3x10^{-54}$ e-value) (Figure 4b). Of those tail fiber proteins, gp43, has an undefined catalytic activity (Mll0443 protein; HMMR; $5.3x10^{-19}$ e-value) and a peptidase S74 domain (HMMER, $7.7x10^{-9}$ e-value). This domain is commonly found in phage endosialidases (polysaccharide depolymerases), where it acts as an intramolecular chaperone[43,44]. It is therefore likely that gp43 functions as an endosialidase and can specifically degrade bacterial polysialic acid on the phage's path to the bacterial cell membrane[45].

Evolved phages derived from the ancestral phages MK and JS (MK.R3-15, MK.R3-30, MK.R84-15, MK.R84-30, MK.R57-15, MK.R57-30) appear to be a recombination of the two. Therefore, to identify SNPs involved in the observed improved phenotypic changes, we focused on the structural gene region (Figure 4c). Only unique SNPs compared to both ancestral phages were considered. This analysis revealed an accumulation of SNPs across five genes, encoding the head-tail joining protein, the tail protein with Baseplate_J domain (HMMR; $5.6x10^{-49}$ e-value) [46], the endosialidase-like tail fiber protein (HMMR; $3.8x10^{-9}$ e-value) [44], the tail fiber assembly protein (HHblits; $5.7x10^{-9}$ e-value) and one structural protein. This structural protein, gp11, shows similarity to a lipase (HMMR; $1x10^{-120}$ e-value) and, consequently, could help the phage hydrolyse encountering lipids (e.g., short-chain fatty acids, long-chain acylglycerols) [47].

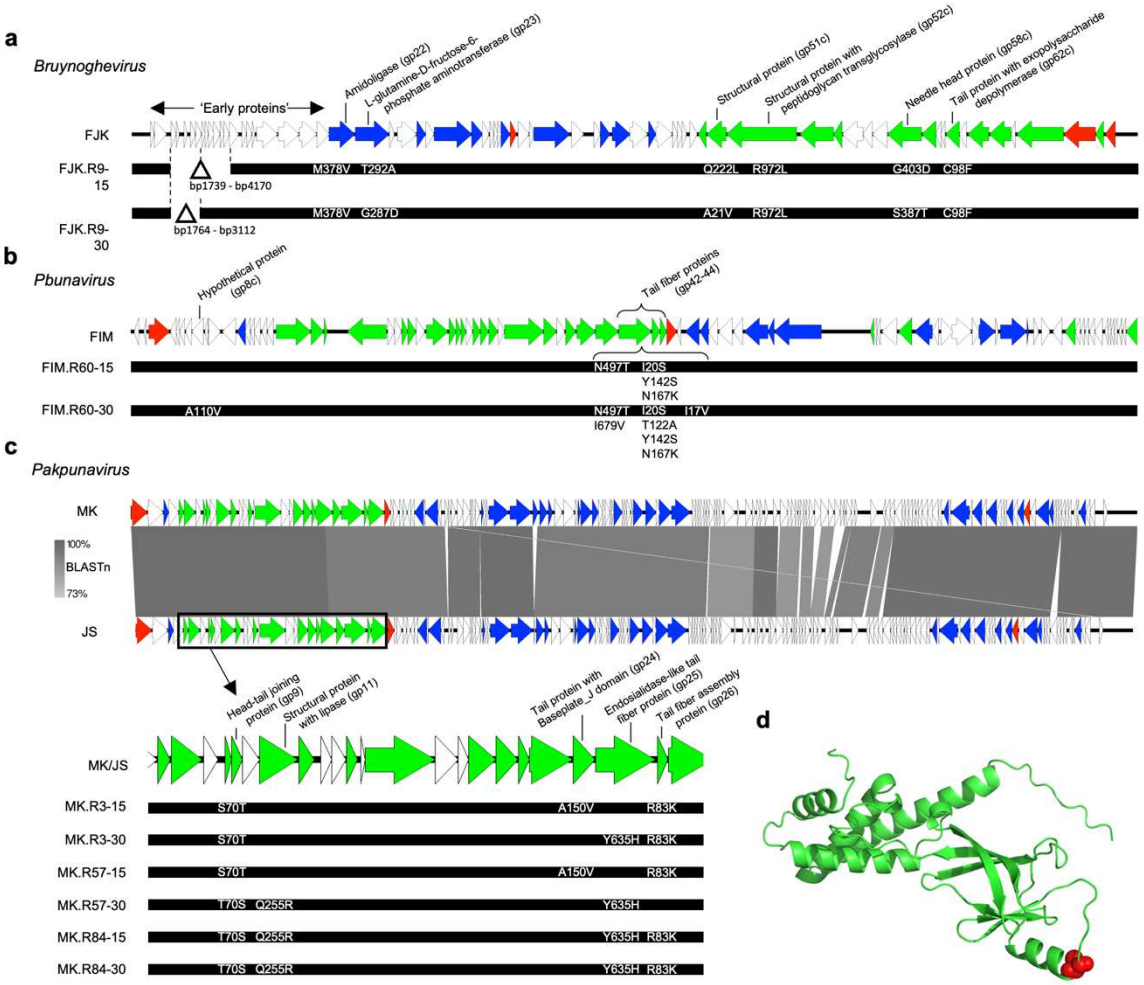

Fig. 4: Schematic genome representation of the evolved phages.

a, **b**, **c**, For each phage genus, a genome map is provided for the ancestral phage (FJK, FIM or MK/JS) with the relevant functional annotations highlighted on top. Each coloured arrow represents a coding sequence with white encoding hypothetical proteins, blue (DNA) metabolism-associated proteins, green virion proteins and red genome packaging or cell lysis proteins. The genomic changes in the evolved phages after round 15 and round 30 are displayed below each ancestral phage genome, with deletions being shown as a delta symbol and the individual SNPs annotated. For the *Pakpunavirus* members, a BLAST comparison between both ancestral phages is also shown. **d**, Tertiary structure prediction of EPS depolymerase FJK_gp62. In red, the cysteine residue on position 98 is highlighted, which is mutated to the aromatic amino acid phenylalanine in the evolved phage.

Impaired bacterial escape from evolved phage predation

Since our above results showed the genotypic improvement of several phage infectivity parameters, we anticipated bacteria to have more trouble escaping phage predation. To investigate this question, we co-incubated planktonic bacterium Paer09 with either ancestral phage FJK or one of the evolved phages (FJK.R9-15/30) for three days. We then sequenced the surviving bacteria, isolated after co-incubation, to identify their mutational changes. Further, we employed soft agar overlay spot assays to examine their susceptibility to the co-incubation phages, as well as phages MK and MK.R3-15 to assess resistance trade-off events observed in preliminary tests (data not shown).

Within the experiment, bacteria developed varying degrees of resistance to the treatment phage, with a high rate of cross-resistance among FJK phages (Figure 5a). Altogether, 43 of the 48 isolates (89.6%) were found to be resistant to phage FJK (n=16, isolates from FJK incubation). For evolved phages FJK.R9-15 (n=17) and FJK.R9-30 (n=15), 25 (52.1%) and 21 (43.8%) resistant isolates were found, respectively. Those 21 FJK.R9-30 resistant isolates showed cross-resistance to FJK.R9-15 and FJK, as demonstrated by Spearman's rank correlation coefficient (r_s) at 0.99 (p=<0.0001) and 0.79 (p=<0.0001), respectively. Bacterial exposure to phage FJK resulted in an immediate optical density increase, whereas phages FJK.R9-15 and FJK.R9-30 suppressed the optical density for 17.4 h and 21.9 h, respectively (Figure 5d, e, f, g). Furthermore, we observed that out of the eight bacterial replicates co-incubated with each phage, both evolved phages had one replicate with a low increase in optical density, reaching 0.3 (FJK.R9-15) and 0.1 (FJK.R9-30) after three days. These values are close to the negative controls (OD_{600} of 0.09) and possibly indicate bacterial eradication.

Among the 48 bacterial isolates, we identified mutations in only six genes (with only one altered gene per mutant), likely conferring resistance to phage predation. Overall, frameshift and nonsense mutations conferred greater resistance against the tested phages than missense variants of the same proteins (Figure 5a). Included among those encoded proteins were all four enzymes (RmlA, RmlB, RmlC and RmlD) involved in the L-rhamnose biosynthesis pathway producing dTDP-L-rhamnose (Figure 5b, c). The majority (52.1%, n=25) of strains had a mutated version of the *rmlA* gene (glucose-1-phosphate thymidylyltransferase). dTDP-L-rhamnose links to the lipopolysaccharides' (LPS) core oligosaccharide to act as the acceptor molecule for the covalent attachment of the A- or B-band O-antigen in *P. aeruginosa*[48,49]. The enzyme involved in this linkage is the alpha-1,3-rhamnosyltransferase (WapR) which was also mutated in several isolates (n=8). Loss of the O-antigen has been associated with a reduced virulence, ineffective swimming and swarming motility and less protection from phagocytosis[50-52]. In one isolate, pslA, part of the Psl biosynthesis pathway, was linked to phage resistance. Psl is essential for biofilm attachment, formation, and differentiation in non-mucoid *P. aeruginosa*[53].

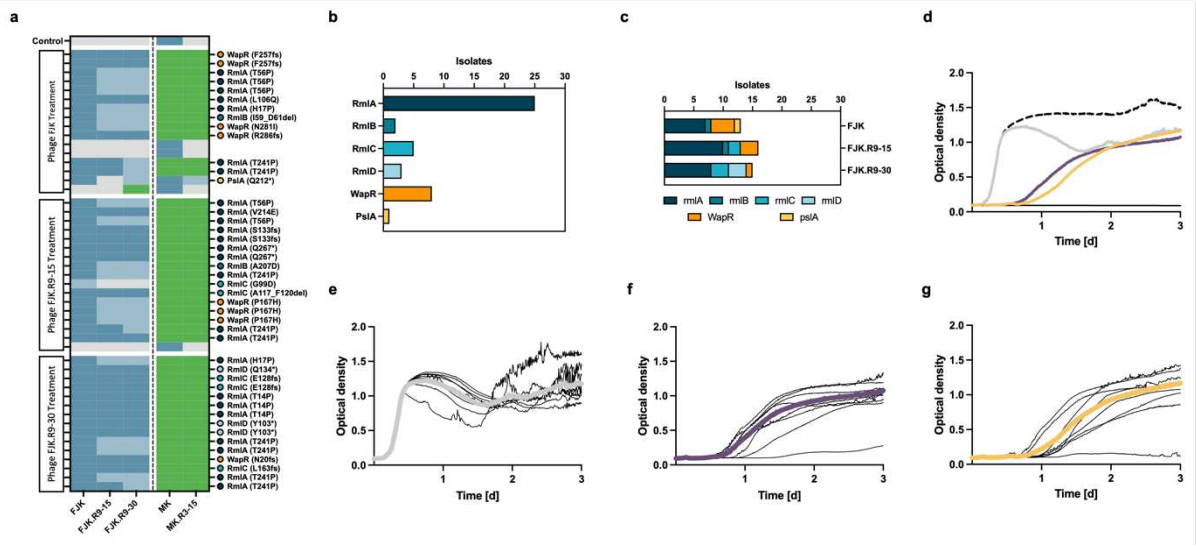

Fig. 5: Phenotypic and genomic characterization of phage-treated Paer09 isolates.

a, Efficacy of plating (EOP) of five phages (FJK, FJK.R9-15, FJK.R9-30, MK, and MK.R3-15) for 48 Paer09 strains treated with individual phages (FJK, FJK.R9-15, FJK.R9-30). The EOP is defined as the concentration ratio of a phage on the phage-treated isolate (numerator) and the naïve Paer09 strain (denominator; Control). An EOP above 10 was considered as "increased" efficiency (green), while an EOP of 0.1 to 10 was ranked as "unchanged" efficiency (grey). A "reduced" efficiency was defined as an EOP between 0.001 and 0.1 (light blue). When no individual plaques were visible or the EOP was equal to or under 0.001 the isolate was determined "resistant" to the phage (blue). Mutation-associated protein of each strain with amino acid change in parentheses. A lack of labelling refers to isolates in which no apparent mutation could be identified. **b**, Illustration of the cumulative number of isolates by mutant protein. **c**, Illustration of the number of isolates by mutant protein according to the treatment group (phage FJK; phage FJK.R9-15; phage FJK.R9-30). **d**, Illustration of the averaged co-incubation curves for phages FJK (grey line), FJK.R9-15 (violet line) and FJK.R9-30 (yellow line) over three days in comparison to a growth control (dotted black line) and negative control (black line). **e**, **f**, **g**, Optical density (OD) measurements of a three-day co-incubation of planktonic naïve Paer09 strain with phage FJK (e), phage FJK.R9-15 (f) and phage FJK.R9-30 (g) at an MOI of 0.001. The thin lines represent each individual replicate (n=8), and the thick coloured line represents the average. For phages FJK.R9-15/30 the completely suppressed replicate was excluded from the average calculation.

We further discovered a resistance trade-off between FJK-phages and MK-phages, illustrated by a negative correlation of susceptibility to phage FJK versus phage MK (r_s=-0.59, p=<0.0001) and MK.R3-15 (r_s=-0.58, p=<0.0001). Accordingly, 43 isolates (89.6%), of which 42 were resistant to phage FJK, had an increased susceptibility towards phage MK (EOP=200 – 3000) and phage MK.R3-15 (EOP=43 – 10714). While the ancestral phage MK was not able to infect the naïve Paer09 strain, its evolved descendant (MK.R3-15) could infect Paer09 with an EOP of 0.00019, compared to its own host strain (Paer03). Among the 48 bacterial isolates, there were five isolates (10.4%; no apparent mutations) showing resistance to phage MK, while no isolate showed resistance to the evolved phage MK.R3-15.

382

383 *Combination of phages to exploit a bacterial phage resistance trade-off*

384

385 Building on this resistance trade-off, we combined FJK.R9-30 and MK.R3-15 into a cocktail.
386 Using optical density monitoring, isothermal microcalorimetry and RT-qPCR, we then
387 compared the cocktails' planktonic and biofilm antimicrobial activity, as well as its antibiofilm
388 efficacy, with the individual phages (Supplementary Table S3). Given the simultaneous
389 antagonistic selective pressures of the cocktail, we anticipated that it would generate improved
390 results in all three dimensions.

391

392 Compared with the individual phage (FJK.R9-30, MOI of 0.001) (Figure 5g), the cocktail could
393 increase the lag time of planktonic Paer09 growth by 565.0% (MOI of 0.001) and 126.5%
394 (MOI of 0.0001) (Figure 6i). While FJK.R9-30 resulted in one replicate (after three days) with
395 an optical density of 0.1, comparable to the negative controls (OD_{600} of 0.09), the cocktail
396 caused two (MOI of 0.0001, OD_{600} 0.09 and 0.1, after three days; Figure 6h) and four (MOI of
397 0.001, OD_{600} 0.08 – 0.09, after seven days; Figure 6g) replicates, to presumably go extinct.

398

399 Regarding the antimicrobial biofilm activity, the co-incubation of Paer09 biofilm with the
400 individual phage MK.R3-15, revealed a heat flow and heat curve like the growth control
401 (Figure 6d, e). In contrast to that, FJK.R9-30 could supress the bacterial heat flow (11.6 µW)
402 and increase the lag time (22.7 h). When we tested the phage cocktail (FJK.R9-30 + MK.R3-
403 15), the minimum heat flow was further reduced to 7.2 µW (p=0.0404). Concordantly, the
404 phage cocktail, with a lag time of 49.8 h, further increased the duration of heat suppression by
405 119.1% (p=0.0051)(Figure 6f). The maximum slope, indicative of the growth rate, was reduced
406 to 0.9 J/h compared with 1.6 J/h (p=0.0056) and 2.1 J/h (p=0.0076) for phage FJK.R9-30 and

the growth control, respectively. At all three tested time points (3, 6 and 24 h), the individual phage FJK.R9-30 presented a higher biofilm cell count reduction than the phage cocktail (Figure 6c).

Isolates retrieved after the co-incubation with the phage cocktail revealed mutations in three proteins (RmlC, WapR and Glycoside hydrolase) (Figure 6a). The isolates incubated with the cocktail did not show any mutations in the *rmlA* gene, the most frequently mutated protein among all isolates treated with the individual phages (Figure 6b). It is noteworthy that none of the eighteen isolates developed a simultaneous resistance to both phages of the phage cocktail.

In conclusion, while the phage cocktail does not have a major impact on the short-term (within the initial 24 h) antibiofilm efficacy compared to the individual phage FJK.R9-30, it exhibits a higher suppressive activity at prolonged incubation times, as bacteria cannot develop full resistance to the phage cocktail.

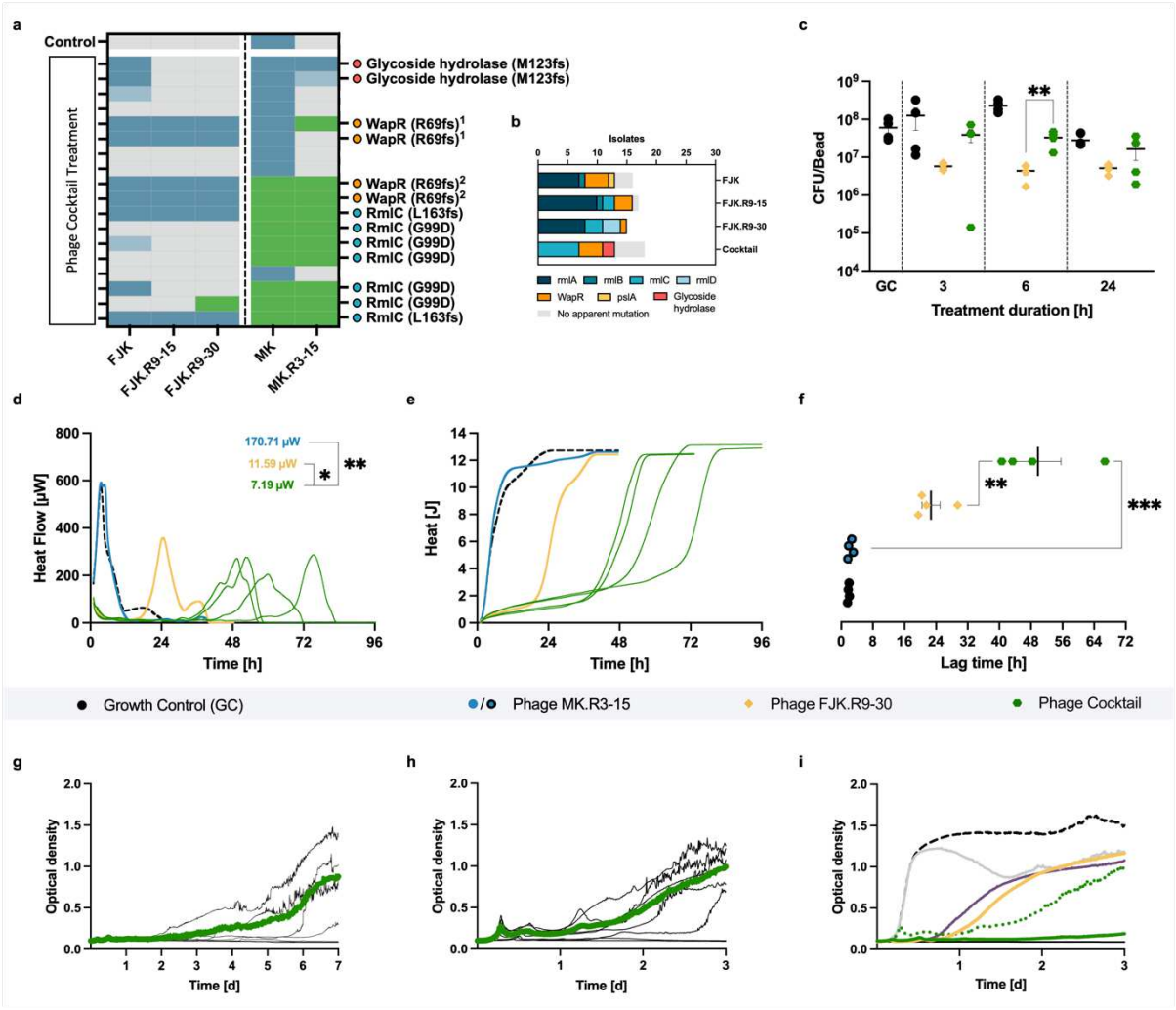

Fig. 6: Antibiofilm and antimicrobial activity of the phage cocktail.

a, Efficacy of plating (EOP) of five phages (FJK, FJK.R9-15, FJK.R9-30, MK, and MK.R3-15) on 18 Paer09 strains treated with the phage cocktail (FJK.R9-30 + MK.R3-15). The EOP is defined as the concentration ratio of a phage on the phage-treated isolate (numerator) and the naïve Paer09 strain (denominator; Control). An EOP above 10 was considered as "increased" efficiency (green), while an EOP of 0.1 to 10 was ranked as "unchanged" efficiency (grey). A "reduced" efficiency was defined as an EOP between 0.001 and 0.1 (light blue). When no individual plaques were visible or the EOP was equal to or under 0.001 the isolate was determined "resistant" to the phage (blue). Mutation-associated protein of each strain with amino acid change in parentheses ([1]c.203_204dupTC p.R69fs and [2]c.205delA p.R69fs). A lack of labelling refers to isolates in which no apparent mutation could be identified. **b**, Illustration of the number of isolates by mutant protein according to the treatment group (phage FJK; phage FJK.R9-15; phage FJK.R9-30; phage Cocktail). **c**, qPCR-determined bacterial load (CFU/bead) of

24 h pre-established Paer09 biofilm without treatment (GC) and after co-incubation (3, 6 and 24 h) with phage FJK.R9-30 (30 rounds of evolution) or the phage cocktail (FJK.R9-30 + MK.R3-15). **d**, **e**, Heat flow (μW) and heat (J) curves measured for 48 h, 72 h and 96 h of Paer09 biofilm co-incubated with phage MK.R3-15 (blue line), phage FJK.R9-30 (yellow line), phage cocktail (FJK.R9-30 + MK.R3-15; individual replicates; green lines) or without phage (GC, dashed black line). Minimum heat flow (μW) values detected in each treated sample are shown on the right (graph d) and relate to the highest suppressive effect of the phage on bacterial cells. **f**, Calculated lag time (h) from the heat (J) curves for each tested condition. **g,** OD measurement of a seven-day co-incubation of planktonic naïve Paer09 strain with the phage cocktail (FJK.R9-30 + MK.R3-15) at an MOI of 0.001. The thin lines represent each individual replicate (n=8), and the thick coloured line represents the average, from which the completely suppressed replicates (n=4) were excluded. **h,** OD measurement of a three-day co-incubation of planktonic naïve Paer09 strain with the phage cocktail (FJK.R9-30 + MK.R3-15) at an MOI of 0.0001. The thin lines represent each individual replicate (n=8), and the thick coloured line represents the average, from which the completely suppressed replicates (n=2) were excluded. **i,** Illustration of all averaged co-incubation curves (including grey, violet, and yellow curves from Fig. 5d) over three days in comparison to a growth control (dotted black line) and negative control (black line). The phage cocktail at an MOI of 0.0001 is shown as a dotted green curve.

All experiments were performed in fourfold and unless specified otherwise, the calorimetric curves (d, e) display the mean. The error bars represent the standard error of the mean. The statistical analysis was conducted by unpaired two-tailed Student's *t* test and *p*-values were indicated by an asterisk (*, p=<0.05; **, p=<0.01; ***, p=<0.001).

Discussion & conclusions

To improve infection management of *P. aeruginosa* biofilms, we developed a directed evolution assay for the combined improvement of the host spectrum, antimicrobial and antibiofilm efficacy, shown for four lytic *P. aeruginosa* phages. These evolved phages reduced the bacterial capacity to escape predation and presumably caused eradication of planktonic

bacterial cultures. The two-phage cocktail based on a bacterial resistance trade-off further exerted a prolonged suppressive activity, likely owing to the absence of bacterial mutants simultaneously resistant to both phages.

Our findings demonstrate that we could successfully direct the improvement of several infectivity parameters for phages from different genera, leading to an improved antimicrobial performance also against a bacterium not included in the evolutionary assay. The results of our study are based on a single directed evolutionary assay, but as previous studies have found, the evolution of phages, given the small genomes and thereby limited evolutionary pathways, demonstrates a great reproducibility down to the codon and nucleotide level[40,54-56]. By contrast, Esvelt *et al.* and Wichman *et al.* highlight how parallel mutations can vary in their order of appearance, resulting in different adaptive trajectories[57,58]. In the end, for Esvelt *et al.* those trajectories converged, stressing the aspect of time (e.g., number of viral generations, rounds) in evolution experiments. In addition, Wichman *et al.* points out that early mutational changes conferring greater boosts in fitness may not always show in all replicates, as those might set them on different adaptation pathways[58].

RT-qPCR allowed us to precisely quantify the antibiofilm degradation capabilities of our phages, providing a starting point for further usage of this technique. Given the problems concerning the treatment of biofilm infections, trained phages, especially phage cocktails, provide an alternative or adjunct to antibiotic chemotherapy[59,60]. The formulation of such cocktails should be based on combining phages that do not interfere with each other and target distinct bacterial receptors[32,61]. In view of this, our resistance-adapted two-phage cocktail prevented the emergence of bacterial resistance and increased bacterial growth suppression beyond 24 h over the use of the individual phage FJK.R9-30. Along those lines, Yang *et al.*

490 composed a five-phage *P. aeruginosa* cocktail (10^9 PFU/ml), comprising two phages that
491 exploit a phage resistance trade-off between the O-antigen and core lipopolysaccharide. Tested
492 against an exponential phase planktonic *P. aeruginosa* PAO1, it took around five days for
493 resistant mutants to arise[62]. In extension to those experiments, our two-phage cocktail at a
494 concentration of approx. 10^3 PFU/ml (MOI of 0.001) showed a continued suppression of
495 planktonic bacteria (clinical isolate Paer09) up to seven days, while no isolated bacterial mutant
496 had developed a dual-phage-resistance. These results highlight possibilities of reapplying the
497 cocktail in a clinical setting until remission of the infection and further emphasizes the
498 importance of a rational phage cocktail design maximizing their clinical applicability.
499
500 However, as the road from bench to bedside is long, several hurdles remain prior to clinical
501 implementation. These include further validations of the evolution platform with different
502 phage-bacteria systems, to reiterate the combined improvement of the infectivity parameters.
503 Thereby these systems are not limited to a specific field, but can cover pathogens relevant to
504 the food industry, aquaculture, or veterinary medicine. Moreover, the platform could also
505 provide insights into evolutionary bacteria-phage interactions, defence strategies and
506 interdependencies, as a realistic biofilm population is employed rather than planktonic bacteria.
507 Identifying the mutational sites of evolutionary adaptation could subsequently serve as a basis
508 for research into phage-bacterial adaptation and aid the identification of targets for genetic
509 engineering, as well as for enzyme-based therapies with depolymerases or lysins[22,28]. At the
510 same time, the platform itself could be further optimized and the optimal number and length of
511 each evolution cycle determined under efficacy and clinical aspects. Considering clinical
512 applications, combinations of evolved phages and antibiotics should be tested against pre-
513 established biofilms to improve treatment efficacy or lower the antibiotic dosage without
514 impairing the outcome. Lastly, those results should then be investigated towards their

translatability from *in vitro* to *in vivo* models, which specifically holds true for the resistance trade-off mechanism[63].

Taken together, this could strengthen phage therapy as a treatment option to improve the outcome of multidrug-resistant bacterial infections with trained resistance-adapted phage cocktails. For personalized medical approaches, phages could be specifically trained against patient strains before administration. Beyond applications in medicine and veterinary medicine, the directed evolution assay could also improve phage efficacy against pathogens relevant in agriculture, aquaculture, and food safety to reduce the amount of antibiotics currently employed[64,65]. All the while, the evolved phages would still be considered as natural, non-genetically engineered entities, limiting the risks if released into the environment and allowing for easier approval[66].

Methods

Collection of Pseudomonas aeruginosa strains

A collection of 80 *P. aeruginosa* clinical isolates was used in this study (Supplementary Data S1). *P. aeruginosa* PAO1 was included as a laboratory reference strain. Bacterial isolates were obtained from hospital and laboratory strain collections in Belgium (n=41), Switzerland (n=17), Italy (n=6) and Germany (n=17). Bacterial stocks were prepared in 20% glycerol and stored at -80 °C until further use. An external diagnostic laboratory (Labor Berlin – Charité Vivantes GmbH, Berlin, Germany) conducted bacterial identification using Vitek2-ID (bioMérieux, Marcy-l'Étoile, France) and MALDI-TOF (bioMérieux, Marcy-l'Étoile, France),

as well as antibiogram analysis using Vitek2-AST (bioMérieux, Marcy-l'Étoile, France) and MICRONAUT-S (MERLIN Diagnostika, Hersel, Germany), including 3- and 4MRGN (multi-resistance Gram-negative) [67-69] classification. Bacteria were propagated at 37 °C using tryptic soy broth (TSB; 3% w/v; USBiological, Salem, USA), tryptic soy agar (TSA; 3% w/v TSB + 1.5% w/v agar) or tryptic soy soft agar (soft agar; 3% w/v TSB + 0.6% w/v agar).

Bacteriophage isolation

Phages were isolated from hospital sewage samples collected in Germany, following a standard enrichment procedure as previously described[70], using *P. aeruginosa* strains isolated from the same hospital. The 0.22 µm-filtered enrichment solutions were subsequently spot tested on soft agar overlays to identify phages. Plaques appearing on the plates were purified by four consecutive single-plaque-passages to ensure phage purity. Next, each isolated phage was produced from a single plaque using either a liquid[71] or solid[72] propagation method. Ultimately, phage lysates were concentrated and purified by PEG 8000 precipitation[73] before storage at 4 °C until further use.

Evolved phages after round 15 and 30 of the evolution assay were isolated by spotting 5 µl tenfold serial dilutions of the corresponding phage mixture on soft agar overlays for each individual bacterial strain in the evolution assay (PAO1, Paer03, Paer09, Paer33, Paer57, Paer60, Paer84 and Paer85). Based on plaque morphology and host strain we identified 31 phages that were purified and produced as described above. Of those, 10 (MK.R3-15, MK.R3-30, MK.R57-15, MK.R57-30, MK.R84-15, MK.R84-30, FIM.R60-15, FIM.R60-30, FJK.R9-15 and FJK.R9-30), representing phages descended from the different ancestral phages

565 determined by BLASTn v2.13.0[74], were concentrated and purified by PEG 8000
566 precipitation[73]. The name is composed of the ancestral phage name (MK, FIM and FJK), the
567 isolation strain (e.g., R84 for Paer84) and the number of passages denoted as 15 (isolation after
568 round 15) or 30 (isolation after round 30).
569
570
571 *Bacteriophage transmission electron microscopy*
572
573 Phage morphology was visualized by transmission electron microscopy (TEM) using negative
574 staining. An aliquot of 15 µl of the phage particle preparation was dropped onto Parafilm prior
575 to the transfer onto a Ni-mesh grid (G2430N; Plano GmbH, Wetzlar, Germany) which has been
576 carbon-coated and glow discharged (Leica MED 020, Leica Microsystems, Wetzlar,
577 Germany). Samples were allowed to adsorb for 10-15 min at room temperature. Grids were
578 washed three times with Aquadest and subsequently treated with 1% aqueous uranyl acetate
579 (SERVA Electrophoresis GmbH, Heidelberg, Germany) for 20 sec for negative staining
580 followed by the removal of excess staining with filter paper before being air dried. Grids were
581 then imaged by TEM using a Zeiss EM 906 microscope (Carl Zeiss Microscopy Deutschland
582 GmbH, Oberkochen, Germany) at a voltage of 80 kV.
583
584
585 *Host range analysis*
586
587 The host range for the ancestral and ten representative evolved phages was determined by soft
588 agar overlay spot assays against the entire collection of *P. aeruginosa* strains.
589

A bacterial overnight culture was mixed (2.5% v/v) with soft agar, poured over TSA and allowed to dry for 10 min. Phage solutions prepared as tenfold dilutions (10^{-1} – 10^{-8}) in 96-well microplates (PN 353072; Corning Inc., Corning, USA) were spotted (5 µl) on the overlays and incubated overnight at 37 °C. Bacterial strains were considered susceptible to a phage when single phage plaques were visible on any of the dilutions. The experiment was either conducted as two biological replicates with two technical replicates each (ancestral phages) or as three biological replicates (evolved phages).

Bacterial biofilm formation and imaging

Bacterial biofilms were formed on autoclaved 4 mm sintered porous glass beads (ROBU® Glasfilter-Geräte GmbH, Hattert, Germany) by incubation in a sterile 24-well plate (Corning Inc., Corning, USA) containing 1 ml TSB inoculated with 1:100 dilution from a one-time use glycerol stock of *P. aeruginosa* and kept at 37 °C and 150 rpm orbital shaking for 24 h under humidity conditions.

For scanning electron microscopy (SEM), glass beads were first dip-washed in phosphate buffered saline (PBS) (Merck KGaA, Darmstadt, Germany) and fixated in a solution of 1% paraformaldehyde and 2.5% glutaraldehyde in 50 mM HEPES for 48 h at room temperature. All samples were subsequently washed in 50 mM HEPES, dehydrated in consecutive steps of 30, 50, 70, 90, 95, 100 and again 100% ethanol, chemically dried overnight in hexamethyldisilazane (Sigma-Aldrich, Darmstadt, Germany), mounted on aluminium stubs, sputter coated with a 16 nm layer of gold-palladium, and examined in the SEM (ZEISS 1530 Gemini, Carl Zeiss Microscopy Deutschland GmbH, Oberkochen, Germany) operating at 3 kV

using the in-lens electron detector. SEM imaging was conducted for one biological replicate of each strain.

In vitro bacteriophage evolution assay

The *in vitro* phage evolution assay consisted of a serial passaging approach with thirty consecutive rounds, inspired by the directed evolution approach of the Appelmans Protocol[75]. For each 24 h round, the undiluted and three tenfold serial dilutions of a mixture of phages were independently co-incubated with 24-h-biofilms of each *P. aeruginosa* strain (PAO1, Paer03, Paer09, Paer33, Paer57, Paer60, Paer84 and Paer85) formed on glass beads. The initial phage mixture comprised equal amounts (10^6 PFU/ml) of the ancestral phages (JS, MK, FIM, and FJK) and after each round of evolution, a new mixture was made, combining all active samples at that round. A schematic illustration of the *in vitro* evolution assay is depicted in figure 1.

The criteria for inclusion of the ancestral phages in the evolution assay were (i) a strictly lytic infection cycle and (ii) phage taxonomy. Four phages from the genera *Pakpunavirus* (MK and JS), *Pbunavirus* (FIM) and *Bruynoghevirus* (FJK) were selected. Inclusion criteria for the bacterial strains were (a) susceptibility to at least one of the ancestral phages, (b) genomic diversity, (c) the antibiotic resistance profile, (d) diversity in biofilm formation (SEM images), and (e) non-auto-plaque former. In total, eight *P. aeruginosa* strains were included in the assay and irrespective of the inclusion criteria, PAO1 was included as a laboratory standard strain.

A 48-channel isothermal microcalorimeter (TAM III; TA Instruments, New Castle, USA) was used to monitor, in real time, the heat produced by each sample in each round, as previously described[76]. Contained in airtight 4 ml disposable glass vials (Waters GmbH, Eschborn, Germany), each sample comprised 450 µl TSB, one in PBS dip-washed 24-h-biofilm glass bead and 50 µl of the corresponding phage mixture dilution. Growth controls without phages were included in each round. Sterility controls, also included in each round, contained TSB, either with (1) the undiluted phage mixture, (2) the undiluted phage mixture and a sterile glass bead or (3) a sterile glass bead.

Active samples were defined based on a reduction in heat (J) of ≥75% compared to the corresponding growth control sample. Active samples and samples containing the undiluted phage mixture across all bacterial strains were pooled into a single mixture after each round. This pooled mixture was centrifuged at 7,000 rpm for 20 min and the supernatant filtered (0.22 µm) before introduction into the next round. During the first fifteen rounds of the evolution assay, the comparative heat reduction analysis was conducted considering the cumulative heat after 24 h, while from round 16 onwards, the cumulative heat from the initial 8 h of the assay were considered.

Throughout the evolution assay the following criteria were applied for each bacterial strain to define which phage-mixture-dilution should be included in the subsequent round:

1. the undiluted phage mixture was kept constant for each round.
2. if at least two of the diluted samples were active – as defined above – all three dilutions were additionally diluted tenfold for the next round.
3. if the three diluted samples were all not active, the dilutions prepared for the next round were diluted one tenth less.

4. if criteria 2 or 3 did not apply, then the tenfold dilutions were not varied for the next round.

At round 0 and after rounds 4, 9, 14, 19, 24 and 29, the pooled phage mixture was serially diluted tenfold and spotted on soft agar overlays of the eight ancestral bacterial strains of the evolution assay. Phage plaques were enumerated after overnight incubation at 37 °C and concentrations in PFU/ml of the phage mixture were determined for each strain. The test was performed in three biological repeats. The calculated phage concentrations were then correlated with the corresponding dilution factors at the onset of rounds 1, 5, 10, 15, 20, 25 and 30, allowing for a direct comparison of the heat production between samples with the same initial phage concentration in the different evolution rounds (Extended Data Figure E2).

Whole genome sequencing and analysis

Total bacterial genomic DNA was extracted using the DNeasy UltraClean Microbial Kit (Qiagen, Hilden, Germany) following the manufacturer's instructions and sequenced as previously described[77]. An Illumina DNA library was prepared using the Nextera Flex Kit (Illumina, San Diego, CA, USA) and sequenced on an Illumina MiniSeq instrument with the MiniSeq High Output Reagent Kit (300 cycles). Additionally, the Rapid Barcoding Kit (Oxford Nanopore Technology, Oxford, UK) was used to prepare the same DNA samples for long-read sequencing on a MinION device using an R9.4.1 flowcell (Oxford Nanopore Technology, Oxford, UK). Guppy v3.1.5 (Oxford Nanopore Technology, Oxford, UK) was used as basecaller. Next, the Unicycler hybrid assembly pipeline v0.4.8.0[78] was performed to assemble the bacterial genomes. The quality of each assembly was visualized with Bandage v0.8.1[79].

Subsequently, the genomes were functionally annotated using Prokka v1.14.6[80]. After determining the core genome (99% ≤ strains ≥ 100%; min. pct. identity for BLASTp: 95) using Roary v3.13.0[81], RAxML v8.2.4[82] was used to infer a maximum likelihood phylogenetic tree of the complete *P. aeruginosa* strain collection, which was then visualised with iTOL v6.5[83]. To analyse the phage treated Paer09 strains' genomic data, single nucleotide polymorphisms (SNP), small deletions and insertions (indels) between the ancestral Paer09 genome and each isolated colony were identified using Snippy v4.6.0[84]. The assembled genomes of all biobank *P. aeruginosa* genomes are available under NCBI BioProject PRJNA906522. For the phage treated Paer09 *P. aeruginosa* genomes, deposited under the accession codes listed in Supplementary Data S4, the Illumina sequencing datasets are available in the Sequence Read Archive (SRA) database via the same BioProject (Reviewer link: https://dataview.ncbi.nlm.nih.gov/object/PRJNA906522?reviewer=abib386262pt1gq09bodbra7fd).

Phage genomes were extracted[85] and the concentration and purity were determined by NanoDrop ND-1000 UV-Vis Spectrophotometer (PEQLAB, Erlangen, Germany). Phage DNA was subsequently sequenced with Illumina as described in Makalatia et al[86]. Phage genomes were assembled using the SPAdes-based PATRIC genome assembly v3.6.12[87], except for phage FJK, FJK.R9-15, FJK.R9-30, FIM, FIM.R60-15 and FIM.R60-30, which were assembled using Shovill v1.1.0[88]. The most similar reference phages were then retrieved using BLASTn v2.13.0[74]. Genome alignment to these identified phages was performed using MEGA11[89]. Resulting aligned phage genomes were functionally annotated through the RASTtk pipeline and manually curated using the BLASTp program v2.13.0[90], HHpred[91], HHblits[92] and HMMER v.3.3[93] integrated in MPI Bioinformatics Toolkit[94]. Genbank files of the ancestral phages were finalized using Artemis v18.1.0[95] and deposited under the accession codes listed in Supplementary Data S2. Illumina reads for both the ancestral and evolved

phages were submitted in the SRA database and are available under NCBI BioProject PRJNA906522 (Reviewer Link: https://dataview.ncbi.nlm.nih.gov/object/PRJNA906522?reviewer=abib386262pt1gq09bodbra7fd). To visualise and illustrate phage genomes, linear comparison figures were generated using Easyfig v2.2.2[96]. To analyse the phages, single nucleotide polymorphisms (SNP), small deletions and insertions (indels) between the ancestral unevolved phages and each evolved phage were identified using Snippy v4.6.0[84] (Supplementary Data S3). The tertiary structure of FJK_gp62 was predicted using ColabFold[97,98]. Similar tertiary structures were identified with DALI[99]. The related TTPA structure was downloaded from the Protein Data Bank (PDB DOI: 10.2210/pdb5mu4/pdb). Protein structures were visualized and analysed using PyMOL 2.5[100,101].

Antibiofilm effect determined by quantitative real-time qPCR

A real-time quantitative polymerase chain reaction (RT-qPCR) was used to quantify the number of viable cells following exposure of 24-h-biofilms of three representative *P. aeruginosa* strains: Paer09, Paer57 (both included in the evolution assay) and Paer36 (not included in the evolution assay) to ancestral and evolved phages isolated at round 15 and 30 by adapting a previously described method[102]. In addition, the antibiofilm activity of combining phages FJK.R9-30 and MK.R3-15 was further investigated on Paer09 biofilms. Briefly, 24-h-biofilms were formed on sterile porous glass beads as described above, dip-washed in 2 ml PBS to remove any planktonic cells and transferred into 48-well plates (LABSOLUTE; Th. Geyer GmbH & Co. KG., Renningen, Germany) containing 450 µl of sterile TSB only (for the growth controls) or with additional 50 µl of phages (for treated samples). Plates were

subsequently incubated at 37 °C and 150 rpm orbital shaking for 3 h, 6 h or 24 h. After incubation, beads where dip-washed in 2 ml PBS, transferred to an Eppendorf tube containing 200 µl of PBS and sonicated (BactoSonic14; BANDELIN, Berlin, Germany) at 200 W_{eff} and 40 kHz for 10 min. Next, the sonicated suspension was used for the DNA extraction of the dislodged biofilm bacterial cells, using the DNeasy UltraClean Microbial Kit (QIAGEN, Hilden, Germany). Extracted bacterial DNA was stored at 4°C until further use.

The NZYTech *Pseudomonas aeruginosa* Real-time PCR Kit targeting the toxin A synthesis regulating gene (RegA) was used according to the manufacturer's instructions (MD02381; NZYTech, Lisboa, Portgual). The extracted DNA was amplified and quantified in the Mastercycler RealPlex^2 (Eppendorf, Hamburg, Germany). In each experiment, as part of the PCR kit, a positive control, negative control, and internal extraction control were included. The experiments were performed as two biological replicates with two technical replicates each. Phage titers (≈1.68 x 10^7 PFU/ml) used for this experiment were determined in biological triplicates on the corresponding bacterial strain, to be tested according to an adapted double agar overlay plaque assay[103].

Antimicrobial activity testing by isothermal microcalorimetry

Isothermal microcalorimetry was used to compare the antimicrobial activity of ancestral and evolved phages isolated at round 15 and 30 against the biofilm of the strains Paer09, Paer36 and Paer57. In addition, the antimicrobial activity of combining phages FJK.R9-30 and MK.R3-15 was further investigated against Paer09 biofilms. The experiments were performed in two biological replicates with two technical replicates each. Phage titers (≈1.68 x 10^7

764 PFU/ml) used for this experiment were determined by an adapted double agar overlay plaque
765 assay[103] in biological triplicates on the corresponding bacterial strain to be tested, except for
766 phage MK.R3-15, determined on Paer03 (≈1.68 x 10^7 PFU/ml) instead of Paer09 in the phage
767 cocktail experiments.
768
769 24-h-biofilms were formed on porous glass beads as described above, dip-washed in 2 ml PBS
770 to remove any planktonic cells and transferred into 4 ml glass vials containing 450 µl of sterile
771 TSB only (for the growth controls) or with an additional 50 µl of phages (for treated samples).
772 Vials were sealed airtight and immediately placed in the calorimeter, where the heat production
773 was monitored during 48 h for single-phage treatment or during 72 h and 96 h for combined-
774 phage treatment.
775
776
777 *Induction, verification, and characterisation of bacteriophage resistant Paer09*
778
779 The co-incubation of the Paer09 strain with either phage FJK, phage FJK.R9-15, phage
780 FJK.R9-30 or the combined phages FJK.R9-30 and MK.R3-15 (cocktail) was performed to
781 induce phage resistance. This experiment was carried out in two biological replicates with four
782 technical replicates (individual phages) or in eight biological replicates (cocktail). Phage titers
783 used in this assay were determined in three biological replicates on the corresponding host
784 strain (Paer09 for phage FJK, FJK.R9-15 and FJK.R9-30 and Paer03 for phage MK.R3-15).
785
786 Paer09 was grown in TSB at 37 °C for 24 h and adjusted to approx. 10^7 CFU/ml (determined
787 in biological triplicates) by dilution in fresh sterile TSB. Then, 160 µl of sterile TSB and 20 µl
788 of bacteria were transferred into a transparent, flat-bottom, 96-well microplate (Corning Inc.,

789 Corning, USA). As growth controls, 20 µl of SM buffer was added. For the treated samples 20
790 µl of phages were applied at a multiplicity of infection (MOI) of 0.001 (approx. 10^3 PFU/ml)
791 and, in case of the phage cocktail, an additional sample with an MOI of 0.0001 (approx. 10^2
792 PFU/ml) was added. The microplate was incubated at 37 °C and 150 rpm orbital shaking for
793 72 h under OD_{600} monitoring (BioTek Epoch 2NSC, Winooski, USA) at 10 min intervals. The
794 cocktail samples at an MOI of 0.001 were incubated for 168 h. The solution from each well
795 was then centrifuged at 10,000 rpm for 1 min and washed three times in PBS, before being
796 plated on TSA. After overnight incubation at 37 °C, based on the replicate (n=32) and distinct
797 morphological appearance, 66 colonies (one replicate, no colonies; one replicate, one colony;
798 twenty-five replicates, two colonies; five replicates, three colonies; from here on referred as
799 "picked-colonies") were picked and re-plated two more times, before being stored as 20%
800 glycerol stocks at -80 °C.
801
802 Phage susceptibility was evaluated for each "picked-colony" (individual biological replicate)
803 and the ancestral Paer09 strain (biological duplicate) by spotting tenfold serial dilutions of the
804 phages (FJK, FJK.R9-15, FJK.R9-30, MK, and MK.R3-15) on soft agar overlays. Phage plaque
805 enumeration was performed after overnight incubation at 37 °C and concentrations were
806 determined as PFU/ml. The relative efficacy of plating (EOP) was defined as the ratio of the
807 phage titer on the "picked-colony" (numerator) and the phage titer on the naïve Paer09 strain
808 (denominator) (Supplementary Data S4) [104]. An EOP above 10 was considered as "increased"
809 efficiency, while an EOP of 0.1 to 10 was ranked as "unchanged" efficiency. A "reduced"
810 efficiency was defined as an EOP between 0.001 and 0.1. When no individual plaques were
811 visible or the EOP was equal to or under 0.001 the isolate was determined "resistant" to the
812 phage[105]. As phage MK was not active on the naïve Paer09 strain, a theoretical value of a single
813 plaque in the undiluted spot ($2x10^3$ PFU/ml) was used in the denominator.

Visualisation and analysis of results

Figure 1 was created with BioRender (BioRender.com). The graphical illustration of the heat, heat flow and optical density graphs was prepared using GraphPad Prism 9 (GraphPad Software, San Diego, USA). For the heat and heat flow curves the experimental replicates were interpolated to a 36 sec equidistant timeline and graphed as mean. By calculating the first derivative of each replicate heat curve (between each point) and the averaged optical density curves (between every second point), the maximum slope and its corresponding tangent were identified. The x-axis value of the intersection point between the baseline and the tangent represents the duration (h) of the lag time[106].

RT-qPCR results were statistically analysed using an unpaired two-tailed Student's *t* test analysis integrated in GraphPad Prism 9. The Spearman's rank correlation coefficient was calculated with all 66 bacterial isolates using GraphPad Prism 9 and reported as r_s with corresponding *p*-value.

Data Availability

The genomic data generated and analysed during the current study is available under NCBI BioProject PRJNA906522 (Reviewer Link: https://dataview.ncbi.nlm.nih.gov/object/PRJNA906522?reviewer=abib386262pt1gq09bodbra7fd).

References

1 Antimicrobial resistance surveillance in Europe 2022 – 2020 data., (WHO Regional Office for Europe/European Centre for Disease Prevention and Control, Copenhagen: WHO Regional Office for Europe, 2022).

2 Antimicrobial resistance in the EU/EEA (EARS-Net) - Annual Epidemiological Report 2021. (European Centre for Disease Prevention and Control, Stockholm: ECDC, 2022).

3 Tacconelli, E. *et al.* Discovery, research, and development of new antibiotics: the WHO priority list of antibiotic-resistant bacteria and tuberculosis. *Lancet Infect Dis* 18, 318-327, doi:10.1016/s1473-3099(17)30753-3 (2018).

4 Centers for Disease, C., Prevention, National Center for Emerging, Z., Infectious Diseases . Division of Healthcare Quality Promotion. Antibiotic Resistance, C. & Strategy, U. Antibiotic resistance threats in the United States, 2019. doi:10.15620/cdc:82532 (2019).

5 Nathwani, D., Raman, G., Sulham, K., Gavaghan, M. & Menon, V. Clinical and economic consequences of hospital-acquired resistant and multidrug-resistant Pseudomonas aeruginosa infections: a systematic review and meta-analysis. *Antimicrob Resist Infect Control* 3, 32, doi:10.1186/2047-2994-3-32 (2014).

6 Pang, Z., Raudonis, R., Glick, B. R., Lin, T.-J. & Cheng, Z. Antibiotic resistance in Pseudomonas aeruginosa: mechanisms and alternative therapeutic strategies. *Biotechnology Advances* 37, 177-192, doi:10.1016/j.biotechadv.2018.11.013 (2019).

7 Langendonk, R. F., Neill, D. R. & Fothergill, J. L. The Building Blocks of Antimicrobial Resistance in Pseudomonas aeruginosa: Implications for Current

Resistance-Breaking Therapies. *Frontiers in Cellular and Infection Microbiology* 11, doi:10.3389/fcimb.2021.665759 (2021).

8 Vert, M. *et al.* Terminology for biorelated polymers and applications (IUPAC Recommendations 2012). *Pure and Applied Chemistry* 84, 377-410, doi:10.1351/PAC-REC-10-12-04 (2012).

9 https://grants.nih.gov/grants/guide/pa-files/PA-06-537.html. (National Institute of Health, 2006).

10 https://grants.nih.gov/grants/guide/pa-files/pa-03-047.html. (National Institute of Health, 2002).

11 Skariyachan, S., Sridhar, V. S., Packirisamy, S., Kumargowda, S. T. & Challapilli, S. B. Recent perspectives on the molecular basis of biofilm formation by Pseudomonas aeruginosa and approaches for treatment and biofilm dispersal. *Folia Microbiologica* 63, 413-432, doi:10.1007/s12223-018-0585-4 (2018).

12 Frølund, B., Palmgren, R., Keiding, K. & Nielsen, P. H. Extraction of extracellular polymers from activated sludge using a cation exchange resin. *Water Research* 30, 1749-1758, doi:10.1016/0043-1354(95)00323-1 (1996).

13 Mann, E. E. & Wozniak, D. J. Pseudomonas biofilm matrix composition and niche biology. *FEMS Microbiology Reviews* 36, 893-916, doi:10.1111/j.1574-6976.2011.00322.x (2012).

14 Thi, M. T. T., Wibowo, D. & Rehm, B. H. A. Pseudomonas aeruginosa Biofilms. *Int J Mol Sci* 21, 8671, doi:10.3390/ijms21228671 (2020).

15 Rasamiravaka, T., Labtani, Q., Duez, P. & El Jaziri, M. The formation of biofilms by Pseudomonas aeruginosa: a review of the natural and synthetic compounds interfering with control mechanisms. *Biomed Res Int* 2015, 759348, doi:10.1155/2015/759348 (2015).

16 Flemming, H.-C. *et al.* Biofilms: an emergent form of bacterial life. *Nature Reviews Microbiology* 14, 563-575, doi:10.1038/nrmicro.2016.94 (2016).

17 Mulcahy, L. R., Isabella, V. M. & Lewis, K. Pseudomonas aeruginosa biofilms in disease. *Microb Ecol* 68, 1-12, doi:10.1007/s00248-013-0297-x (2014).

18 Fong, S. A. *et al.* Activity of Bacteriophages in Removing Biofilms of Pseudomonas aeruginosa Isolates from Chronic Rhinosinusitis Patients. *Frontiers in cellular and infection microbiology* 7, 418-418, doi:10.3389/fcimb.2017.00418 (2017).

19 Forti, F. *et al.* Design of a Broad-Range Bacteriophage Cocktail That Reduces Pseudomonas aeruginosa Biofilms and Treats Acute Infections in Two Animal Models. *Antimicrob Agents Chemother* 62, e02573-02517, doi:10.1128/AAC.02573-17 (2018).

20 Yan, J., Mao, J. & Xie, J. Bacteriophage Polysaccharide Depolymerases and Biomedical Applications. *BioDrugs* 28, 265-274, doi:10.1007/s40259-013-0081-y (2014).

21 Glonti, T., Chanishvili, N. & Taylor, P. W. Bacteriophage-derived enzyme that depolymerizes the alginic acid capsule associated with cystic fibrosis isolates of Pseudomonas aeruginosa. *Journal of Applied Microbiology* 108, 695-702, doi:10.1111/j.1365-2672.2009.04469.x (2010).

22 Olszak, T. *et al.* The O-specific polysaccharide lyase from the phage LKA1 tailspike reduces Pseudomonas virulence. *Sci Rep* 7, 16302, doi:10.1038/s41598-017-16411-4 (2017).

23 Knecht, L. E., Veljkovic, M. & Fieseler, L. Diversity and Function of Phage Encoded Depolymerases. *Frontiers in Microbiology* 10, doi:10.3389/fmicb.2019.02949 (2020).

24 Mi, L. *et al.* Identification of a lytic Pseudomonas aeruginosa phage depolymerase and its anti-biofilm effect and bactericidal contribution to serum. *Virus Genes* 55, 394-405, doi:10.1007/s11262-019-01660-4 (2019).

914 25 Guo, M. *et al.* A Novel Antimicrobial Endolysin, LysPA26, against Pseudomonas
915 aeruginosa. *Frontiers in Microbiology* 8, doi:10.3389/fmicb.2017.00293 (2017).
916 26 Hanlon, G. W., Denyer, S. P., Olliff, C. J. & Ibrahim, L. J. Reduction in
917 exopolysaccharide viscosity as an aid to bacteriophage penetration through
918 Pseudomonas aeruginosa biofilms. *Appl Environ Microbiol* 67, 2746-2753,
919 doi:10.1128/AEM.67.6.2746-2753.2001 (2001).
920 27 Pires, D. P., Oliveira, H., Melo, L. D. R., Sillankorva, S. & Azeredo, J. Bacteriophage-
921 encoded depolymerases: their diversity and biotechnological applications. *Applied*
922 *Microbiology and Biotechnology* 100, 2141-2151, doi:10.1007/s00253-015-7247-0
923 (2016).
924 28 Latka, A., Maciejewska, B., Majkowska-Skrobek, G., Briers, Y. & Drulis-Kawa, Z.
925 Bacteriophage-encoded virion-associated enzymes to overcome the carbohydrate
926 barriers during the infection process. *Applied Microbiology and Biotechnology* 101,
927 3103-3119, doi:10.1007/s00253-017-8224-6 (2017).
928 29 Visnapuu, A., Van der Gucht, M., Wagemans, J. & Lavigne, R. Deconstructing the
929 Phage-Bacterial Biofilm Interaction as a Basis to Establish New Antibiofilm Strategies.
930 *Viruses* 14, doi:10.3390/v14051057 (2022).
931 30 Pearl, S., Gabay, C., Kishony, R., Oppenheim, A. & Balaban, N. Q. Nongenetic
932 Individuality in the Host–Phage Interaction. *PLOS Biology* 6, e120,
933 doi:10.1371/journal.pbio.0060120 (2008).
934 31 Chan, B. K., Abedon, S. T. & Loc-Carrillo, C. Phage cocktails and the future of phage
935 therapy. *Future Microbiol* 8, 769-783, doi:10.2217/fmb.13.47 (2013).
936 32 Merabishvili, M., Pirnay, J.-P. & De Vos, D. in *Bacteriophage Therapy: From Lab to*
937 *Clinical Practice* (eds Joana Azeredo & Sanna Sillankorva) 99-110 (Springer New
938 York, 2018).

939 33 Abedon, S. T., Danis-Wlodarczyk, K. M. & Wozniak, D. J. Phage Cocktail
940 Development for Bacteriophage Therapy: Toward Improving Spectrum of Activity
941 Breadth and Depth. *Pharmaceuticals (Basel)* 14, doi:10.3390/ph14101019 (2021).
942 34 Borin, J. M., Avrani, S., Barrick, J. E., Petrie, K. L. & Meyer, J. R. Coevolutionary
943 phage training leads to greater bacterial suppression and delays the evolution of phage
944 resistance. *Proceedings of the National Academy of Sciences* 118, e2104592118,
945 doi:10.1073/pnas.2104592118 (2021).
946 35 Betts, A., Vasse, M., Kaltz, O. & Hochberg, M. E. Back to the future: evolving
947 bacteriophages to increase their effectiveness against the pathogen Pseudomonas
948 aeruginosa PAO1. *Evol Appl* 6, 1054-1063, doi:10.1111/eva.12085 (2013).
949 36 Burmeister, A. R., Sullivan, R. M., Gallie, J. & Lenski, R. E. Sustained coevolution of
950 phage Lambda and Escherichia coli involves inner- as well as outer-membrane defences
951 and counter-defences. *Microbiology (Reading)* 167, doi:10.1099/mic.0.001063 (2021).
952 37 Mapes, A. C., Trautner, B. W., Liao, K. S. & Ramig, R. F. Development of expanded
953 host range phage active on biofilms of multi-drug resistant Pseudomonas aeruginosa.
954 *Bacteriophage* 6, e1096995, doi:10.1080/21597081.2015.1096995 (2016).
955 38 Favor, A. H., Llanos, C. D., Youngblut, M. D. & Bardales, J. A. Optimizing
956 bacteriophage engineering through an accelerated evolution platform. *Scientific*
957 *Reports* 10, 13981, doi:10.1038/s41598-020-70841-1 (2020).
958 39 Kering, K. K., Zhang, X., Nyaruaba, R., Yu, J. & Wei, H. Application of Adaptive
959 Evolution to Improve the Stability of Bacteriophages during Storage. *Viruses* 12,
960 doi:10.3390/v12040423 (2020).
961 40 Akusobi, C., Chan, B. K., Williams, E., Wertz, J. E. & Turner, P. E. Parallel Evolution
962 of Host-Attachment Proteins in Phage PP01 Populations Adapting to Escherichia coli
963 O157:H7. *Pharmaceuticals (Basel)* 11, doi:10.3390/ph11020060 (2018).

964 41 Swanson, N. A. *et al.* Cryo-EM structure of the periplasmic tunnel of T7 DNA-
965 ejectosome at 2.7 Å resolution. *Mol Cell* 81, 3145-3159.e3147,
966 doi:10.1016/j.molcel.2021.06.001 (2021).
967 42 Pyra, A. *et al.* Tail tubular protein A: a dual-function tail protein of Klebsiella
968 pneumoniae bacteriophage KP32. *Scientific Reports* 7, 2223, doi:10.1038/s41598-017-
969 02451-3 (2017).
970 43 Schwarzer, D., Stummeyer, K., Gerardy-Schahn, R. & Mühlenhoff, M.
971 Characterization of a Novel Intramolecular Chaperone Domain Conserved in
972 Endosialidases and Other Bacteriophage Tail Spike and Fiber Proteins *<sup>
973 </sup>. *Journal of Biological Chemistry* 282, 2821-2831,
974 doi:10.1074/jbc.M609543200 (2007).
975 44 Morley, T. J., Willis, L. M., Whitfield, C., Wakarchuk, W. W. & Withers, S. G. A new
976 sialidase mechanism: bacteriophage K1F endo-sialidase is an inverting glycosidase. *J*
977 *Biol Chem* 284, 17404-17410, doi:10.1074/jbc.M109.003970 (2009).
978 45 Jakobsson, E., Schwarzer, D., Jokilammi, A. & Finne, J. Endosialidases: Versatile
979 Tools for the Study of Polysialic Acid. *Top Curr Chem* 367, 29-73,
980 doi:10.1007/128_2012_349 (2015).
981 46 Haggård-Liungquist, E. *et al.* Bacteriophage P2: Genes Involved in Baseplate
982 Assembly. *Virology* 213, 109-121, doi:10.1006/viro.1995.1551 (1995).
983 47 Gil, F. *et al.* The lytic cassette of mycobacteriophage Ms6 encodes an enzyme with
984 lipolytic activity. *Microbiology (Reading)* 154, 1364-1371,
985 doi:10.1099/mic.0.2007/014621-0 (2008).
986 48 Poon, K. K. H., Westman, E. L., Vinogradov, E., Jin, S. & Lam, J. S. Functional
987 characterization of MigA and WapR: putative rhamnosyltransferases involved in outer

core oligosaccharide biosynthesis of Pseudomonas aeruginosa. *J Bacteriol* 190, 1857-1865, doi:10.1128/JB.01546-07 (2008).

49 Rahim, R., Burrows, L. L., Monteiro, M. A., Perry, M. B. & Lam, J. S. Involvement of the rml locus in core oligosaccharide and O polysaccharide assembly in Pseudomonas aeruginosa. *Microbiology* 146, 2803-2814, doi:10.1099/00221287-146-11-2803 (2000).

50 Elamin, A. A. *et al.* Novel drug targets in cell wall biosynthesis exploited by gene disruption in Pseudomonas aeruginosa. *PLoS One* 12, e0186801, doi:10.1371/journal.pone.0186801 (2017).

51 Alphey, M. S. *et al.* Allosteric Competitive Inhibitors of the Glucose-1-phosphate Thymidylyltransferase (RmlA) from Pseudomonas aeruginosa. *ACS Chemical Biology* 8, 387-396, doi:10.1021/cb300426u (2013).

52 Huszczynski, S. M., Lam, J. S. & Khursigara, C. M. The Role of Pseudomonas aeruginosa Lipopolysaccharide in Bacterial Pathogenesis and Physiology. *Pathogens* 9, doi:10.3390/pathogens9010006 (2019).

53 Overhage, J., Schemionek, M., Webb, J. S. & Rehm, B. H. A. Expression of the psl operon in Pseudomonas aeruginosa PAO1 biofilms: PslA performs an essential function in biofilm formation. *Appl Environ Microbiol* 71, 4407-4413, doi:10.1128/AEM.71.8.4407-4413.2005 (2005).

54 Sackman, A. M. *et al.* Mutation-Driven Parallel Evolution during Viral Adaptation. *Mol Biol Evol* 34, 3243-3253, doi:10.1093/molbev/msx257 (2017).

55 Perry, E. B., Barrick, J. E. & Bohannan, B. J. The Molecular and Genetic Basis of Repeatable Coevolution between Escherichia coli and Bacteriophage T3 in a Laboratory Microcosm. *PLoS One* 10, e0130639, doi:10.1371/journal.pone.0130639 (2015).

1013 56 Bull, J. J. *et al.* Exceptional convergent evolution in a virus. *Genetics* 147, 1497-1507,
1014 doi:10.1093/genetics/147.4.1497 (1997).
1015 57 Esvelt, K. M., Carlson, J. C. & Liu, D. R. A system for the continuous directed evolution
1016 of biomolecules. *Nature* 472, 499-503, doi:10.1038/nature09929 (2011).
1017 58 Wichman, H. A., Badgett, M. R., Scott, L. A., Boulianne, C. M. & Bull, J. J. Different
1018 Trajectories of Parallel Evolution During Viral Adaptation. *Science* 285, 422-424,
1019 doi:10.1126/science.285.5426.422 (1999).
1020 59 Łusiak-Szelachowska, M., Weber-Dąbrowska, B. & Górski, A. Bacteriophages and
1021 Lysins in Biofilm Control. *Virol Sin* 35, 125-133, doi:10.1007/s12250-019-00192-3
1022 (2020).
1023 60 Eskenazi, A. *et al.* Combination of pre-adapted bacteriophage therapy and antibiotics
1024 for treatment of fracture-related infection due to pandrug-resistant Klebsiella
1025 pneumoniae. *Nature Communications* 13, 302, doi:10.1038/s41467-021-27656-z
1026 (2022).
1027 61 Gordillo Altamirano, F. L. & Barr, J. J. Unlocking the next generation of phage therapy:
1028 the key is in the receptors. *Current Opinion in Biotechnology* 68, 115-123,
1029 doi:10.1016/j.copbio.2020.10.002 (2021).
1030 62 Yang, Y. *et al.* Development of a Bacteriophage Cocktail to Constrain the Emergence
1031 of Phage-Resistant Pseudomonas aeruginosa. *Front Microbiol* 11, 327,
1032 doi:10.3389/fmicb.2020.00327 (2020).
1033 63 Castledine, M. *et al.* Parallel evolution of Pseudomonas aeruginosa phage resistance
1034 and virulence loss in response to phage treatment in vivo and in vitro. *Elife* 11,
1035 doi:10.7554/eLife.73679 (2022).
1036 64 Sharma, S. *et al.* Bacteriophages and its applications: an overview. *Folia*
1037 *Microbiologica* 62, 17-55, doi:10.1007/s12223-016-0471-x (2017).

65 Połaska, M. & Sokołowska, B. Bacteriophages-a new hope or a huge problem in the food industry. *AIMS Microbiol* 5, 324-346, doi:10.3934/microbiol.2019.4.324 (2019).

66 Nair, A. & Khairnar, K. Genetically engineered phages for therapeutics: proceed with caution. *Nature Medicine* 25, 1028-1028, doi:10.1038/s41591-019-0506-3 (2019).

67 [Hygiene requirements for the reprocessing of medical devices. Recommendation of the Commission for Hospital Hygiene and Infection Prevention (KRINKO) at the Robert Koch Institute (RKI) and the Federal Institute for Drugs and Medical Devices (BfArM)]. *Bundesgesundheitsblatt Gesundheitsforschung Gesundheitsschutz* 55, 1244-1310, doi:10.1007/s00103-012-1548-6 (2012).

68 KRINKO. Ergänzung zur Empfehlung der KRINKO „Hygienemaßnahmen bei Infektionen oder Besiedlung mit multiresistenten gramnegativen Stäbchen“ (2012) im Zusammenhang mit der von EUCAST neu definierten Kategorie „I“ bei der Antibiotikaresistenzbestimmung: Konsequenzen für die Definition von MRGN. *Epidemiologisches Bulletin*, 82--83, doi:10.25646/5916 (2019).

69 Wolfensberger, A., Kuster, S. P., Marchesi, M., Zbinden, R. & Hombach, M. The effect of varying multidrug-resistence (MDR) definitions on rates of MDR gram-negative rods. *Antimicrob Resist Infect Control* 8, 193, doi:10.1186/s13756-019-0614-3 (2019).

70 Wang, L., Tkhilaishvili, T., Bernal Andres, B., Trampuz, A. & Gonzalez Moreno, M. Bacteriophage-antibiotic combinations against ciprofloxacin/ceftriaxone-resistant Escherichia coli in vitro and in an experimental Galleria mellonella model. *Int J Antimicrob Agents* 56, 106200, doi:10.1016/j.ijantimicag.2020.106200 (2020).

71 Kunisch, F. & Gonzalez Moreno, M. (Protocol Exchange, PROTOCOL (Version 1) available at [https://doi.org/10.21203/rs.3.pex-1886/v1], 2023).

72 Kunisch, F., Ponce Benavente, L. & Gonzalez Moreno, M. (Protocol Exchange, PROTOCOL (Version 1) available at [https://doi.org/10.21203/rs.3.pex-1953/v1], 2023).

73 Kunisch, F., Wagemans, J. & Gonzalez Moreno, M. (Protocol Exchange, PROTOCOL (Version 1) available at [https://doi.org/10.21203/rs.3.pex-1956/v1], 2023).

74 Zhang, Z., Schwartz, S., Wagner, L. & Miller, W. A greedy algorithm for aligning DNA sequences. *J Comput Biol* 7, 203-214, doi:10.1089/10665270050081478 (2000).

75 Burrowes, B. H., Molineux, I. J. & Fralick, J. A. Directed in Vitro Evolution of Therapeutic Bacteriophages: The Appelmans Protocol. *Viruses* 11, 241, doi:10.3390/v11030241 (2019).

76 Butini, M. E. *et al.* in *Advances in Microbiology, Infectious Diseases and Public Health: Volume 13* (ed Gianfranco Donelli) 61-77 (Springer International Publishing, 2019).

77 Lood, C. *et al.* Genomics of an endemic cystic fibrosis Burkholderia multivorans strain reveals low within-patient evolution but high between-patient diversity. *PLOS Pathogens* 17, e1009418, doi:10.1371/journal.ppat.1009418 (2021).

78 Wick, R. R., Judd, L. M., Gorrie, C. L. & Holt, K. E. Unicycler: resolving bacterial genome assemblies from short and long sequencing reads. *bioRxiv*, 096412, doi:10.1101/096412 (2016).

79 Wick, R. R., Schultz, M. B., Zobel, J. & Holt, K. E. Bandage: interactive visualization of de novo genome assemblies. *Bioinformatics* 31, 3350-3352, doi:10.1093/bioinformatics/btv383 (2015).

80 Seemann, T. Prokka: rapid prokaryotic genome annotation. *Bioinformatics* 30, 2068-2069, doi:10.1093/bioinformatics/btu153 (2014).

1086 81 Page, A. J. *et al.* Roary: rapid large-scale prokaryote pan genome analysis.
1087 *Bioinformatics* 31, 3691-3693, doi:10.1093/bioinformatics/btv421 (2015).
1088 82 Stamatakis, A. RAxML version 8: a tool for phylogenetic analysis and post-analysis of
1089 large phylogenies. *Bioinformatics* 30, 1312-1313, doi:10.1093/bioinformatics/btu033
1090 (2014).
1091 83 Letunic, I. & Bork, P. Interactive Tree Of Life (iTOL) v4: recent updates and new
1092 developments. *Nucleic Acids Res* 47, W256-w259, doi:10.1093/nar/gkz239 (2019).
1093 84 Seemann, T. (GitHub, https://github.com/tseemann/snippy, 2015).
1094 85 Kunisch, F., Wagemans, J. & Gonzalez Moreno, M. (Protocol Exchange,
1095 PROTOCOL (Version 1) available at [https://doi.org/10.21203/rs.3.pex-1955/v1],
1096 2023).
1097 86 Makalatia, K. *et al.* Characterization of Salmonella Isolates from Various Geographical
1098 Regions of the Caucasus and Their Susceptibility to Bacteriophages. *Viruses* 12,
1099 doi:10.3390/v12121418 (2020).
1100 87 Bankevich, A. *et al.* SPAdes: a new genome assembly algorithm and its applications to
1101 single-cell sequencing. *J Comput Biol* 19, 455-477, doi:10.1089/cmb.2012.0021
1102 (2012).
1103 88 Seemann, T. (GitHub, https://github.com/tseemann/shovill, 2017).
1104 89 Tamura, K., Stecher, G. & Kumar, S. MEGA11: Molecular Evolutionary Genetics
1105 Analysis Version 11. *Molecular Biology and Evolution* 38, 3022-3027,
1106 doi:10.1093/molbev/msab120 (2021).
1107 90 Altschul, S. F. *et al.* Gapped BLAST and PSI-BLAST: a new generation of protein
1108 database search programs. *Nucleic Acids Research* 25, 3389-3402,
1109 doi:10.1093/nar/25.17.3389 (1997).

91 Söding, J., Biegert, A. & Lupas, A. N. The HHpred interactive server for protein homology detection and structure prediction. *Nucleic Acids Res* 33, W244-248, doi:10.1093/nar/gki408 (2005).

92 Remmert, M., Biegert, A., Hauser, A. & Söding, J. HHblits: lightning-fast iterative protein sequence searching by HMM-HMM alignment. *Nature Methods* 9, 173-175, doi:10.1038/nmeth.1818 (2012).

93 Wheeler, T. J. & Eddy, S. R. nhmmer: DNA homology search with profile HMMs. *Bioinformatics* 29, 2487-2489, doi:10.1093/bioinformatics/btt403 (2013).

94 Gabler, F. *et al.* Protein Sequence Analysis Using the MPI Bioinformatics Toolkit. *Curr Protoc Bioinformatics* 72, e108, doi:10.1002/cpbi.108 (2020).

95 Rutherford, K. *et al.* Artemis: sequence visualization and annotation. *Bioinformatics* 16, 944-945, doi:10.1093/bioinformatics/16.10.944 (2000).

96 Sullivan, M. J., Petty, N. K. & Beatson, S. A. Easyfig: a genome comparison visualizer. *Bioinformatics* 27, 1009-1010, doi:10.1093/bioinformatics/btr039 (2011).

97 Mirdita, M. *et al.* ColabFold - Making protein folding accessible to all. *bioRxiv*, 2021.2008.2015.456425, doi:10.1101/2021.08.15.456425 (2022).

98 Jumper, J. *et al.* Highly accurate protein structure prediction with AlphaFold. *Nature* 596, 583-589, doi:10.1038/s41586-021-03819-2 (2021).

99 Holm, L. DALI and the persistence of protein shape. *Protein Science* 29, 128-140, doi:10.1002/pro.3749 (2020).

100 DeLano, W. in *Abstracts of Papers of the American Chemical Society.* U313-U314 (AMER CHEMICAL SOC 1155 16TH ST, NW, WASHINGTON, DC 20036 USA).

101 PyMOL v. 2.5 (http://www.pymol.org/pymol, 2020).

102 Liu, H., Niu, Y. D., Li, J., Stanford, K. & McAllister, T. A. Rapid and Accurate Detection of Bacteriophage Activity against *Escherichia coli* O157:H7 by Propidium

Monoazide Real-Time PCR. *BioMed Research International* 2014, 319351, doi:10.1155/2014/319351 (2014).

103 Kropinski, A. M., Mazzocco, A., Waddell, T. E., Lingohr, E. & Johnson, R. P. Enumeration of bacteriophages by double agar overlay plaque assay. *Methods Mol Biol* 501, 69-76, doi:10.1007/978-1-60327-164-6_7 (2009).

104 Abedon, S. T. & Katsaounis, T. I. Basic Phage Mathematics. *Methods Mol Biol* 1681, 3-30, doi:10.1007/978-1-4939-7343-9_1 (2018).

105 Viazis, S., Akhtar, M., Feirtag, J., Brabban, A. D. & Diez-Gonzalez, F. Isolation and characterization of lytic bacteriophages against enterohaemorrhagic Escherichia coli. *Journal of Applied Microbiology* 110, 1323-1331, doi:10.1111/j.1365-2672.2011.04989.x (2011).

106 Howell, M., Wirz, D., Daniels, A. U. & Braissant, O. Application of a Microcalorimetric Method for Determining Drug Susceptibility in Mycobacterium Species. *Journal of Clinical Microbiology* 50, 16-20, doi:10.1128/JCM.05556-11 (2012).

Extended Data

Extended Data is available for this paper.

Supplementary Information

Supplementary Information is available for this paper.

Supplementary Files

This is a list of supplementary files associated with this preprint. Click to download.

- NCOMMS2323549TDBPRSupplementaryInformation.xlsx
- NCOMMS2323549TDBPRExtendedData.pdf
- NCOMMS2323549TRS.pdf